First-in-class anti-human CD45RC antibody targets CD45RChigh T and B cells to mitigate pathogenic immune responses

Cécile Bergua, Ghenima Ahmil-Boiteau, Laure-Hélène Ouisse, Nadège Vimond, Céline Sérazin, Lisa Dugast, Romain Humeau, Apolline Salama, Laurent Tesson, Katleen Swinnen, et al.

Molecular Therapy
Original Article

First-in-class anti-human CD45RC antibody targets CD45RC^{high} T and B cells to mitigate pathogenic immune responses

Cécile Bergua,[1] Ghenima Ahmil-Boiteau,[2] Laure-Hélène Ouisse,[2] Nadège Vimond,[1] Céline Sérazin,[2] Lisa Dugast,[1] Romain Humeau,[2] Apolline Salama,[2] Laurent Tesson,[2] Katleen Swinnen,[1] Ronald Van Brempt,[1] Alexis Collette,[1] Ignacio Anegon,[2,3] and Carole Guillonneau[1,2,3]

[1]AbolerIS Pharma, Nantes, France; [2]Nantes Université, INSERM, Center for Research in Transplantation and Translational Immunology, UMR 1064, CNRS, Nantes, France

CD45RC, an isoform of the transmembrane tyrosine phosphatase CD45, regulates T and B cell antigen receptor signaling and is highly expressed on Th1 precursors, Th1 cells, T effector memory CD45RA$^+$ cells, and most B cells. Preclinical studies have shown that anti-CD45RC monoclonal antibodies (mAbs) can prevent or control diseases such as transplant rejection, graft-versus-host disease (GvHD), Duchenne muscular dystrophy (DMD), and autoimmune polyendocrinopathy-candidiasis-ectodermal dystrophy (APECED or APS-1). However, their mechanism of action remained unclear. Here, we elucidate the mechanism of anti-human CD45RC mAbs, showing that it selectively induces apoptosis in CD45RC^{high} T and B cells through binding to cells expressing >24 CD45RC molecules/µm^2. This interaction triggers intracellular signaling without cytokine release. Cytotoxicity by apoptosis is enhanced by cross-linking with a secondary antibody. The mAb also promotes antibody-dependent cellular phagocytosis by monocyte-derived macrophages, without inducing antibody-dependent cellular cytotoxicity or complement-dependent cytotoxicity, likely due to the length of CD45RC. In CD34$^+$-humanized NSG mice, anti-CD45RC mAbs demonstrated dose-dependent depletion of CD45RC^{high} T and B cells and defined a minimum effective dose to prevent xenogeneic GvHD. These findings define the mechanism of action of this first-in-class anti-human CD45RC therapeutic mAb and supports its potential for the treatment of transplant rejection, GvHD, and autoimmune diseases.

INTRODUCTION

Dysregulation of the T effector (Teff)/T regulatory (Treg) cell balance, along with the activation of autoreactive or alloreactive B cells producing pathogenic antibodies, is a hallmark of autoimmune diseases or transplant rejection. These mechanisms underlie the poor prognosis associated with many such conditions.[1–5] Current therapeutic strategies, including anti-CD20 and anti-CD3 monoclonal antibodies (mAbs), have improved outcomes, but efficacy, persistence of effects, and toxicity issues remain unaddressed. Many patients either fail to respond or relapse, potentially due to the narrow targeting of these therapies, which often focus solely on either the T or the B cell arm.[6,7] Additionally, long-term immune tolerance hinges on the activation and maintenance of Treg cells. Despite advancements, existing treatments frequently fail to achieve durable immune regulation due to their limited specificity, systemic side effects, or inability to simultaneously address multiple pathogenic pathways. This underscores the urgent need for novel, targeted therapies capable of eliminating harmful immune populations while preserving Treg and memory cells to promote immune tolerance and protection against pathogens.

The CD45RC protein (comprising the CD45RABC and CD45RBC protein isoforms expressing the C domain) has emerged as an attractive target for antibody-based therapy. The CD45RC protein is a type 1 transmembrane receptor protein tyrosine phosphatase that plays a pivotal role in regulating T and B cell activation by modulating receptor signaling. CD45RC is highly expressed (CD45RC^{high}) on most blood B cells, including plasmablasts, mature natural killer (NK) cells, plasmacytoid dendritic cells (pDCs) and type 2 innate lymphoid cells (ILC2). Within the T cell lineage, CD45RC expression is restricted to type 1 T helper (Th1) precursors, Th1 cells, and terminally differentiated effector memory RA$^+$ (TEMRA) T cells.[8–12] In contrast, Treg cells, certain memory T cells, such as the one involved in viral immunity, and thymocytes exhibit low or absent CD45RC expression (CD45RC$^{low/neg}$). CD45RC is also absent on CD34$^+$ stem cells, polymorphonuclear leukocytes (PMNs), most monocytes,

Received 28 March 2025; accepted 28 October 2025;
https://doi.org/10.1016/j.ymthe.2025.10.057.

[3]Senior author

Correspondence: Carole Guillonneau, Nantes Université, INSERM, Center for Research in Transplantation and Translational Immunology, UMR 1064, CNRS, Nantes, France.
E-mail: carole.guillonneau@univ-nantes.fr
Correspondence: Ignacio Anegon, Nantes Université, INSERM, Center for Research in Transplantation and Translational Immunology, UMR 1064, CNRS, Nantes, France.
E-mail: ianegon@nantes.inserm.fr

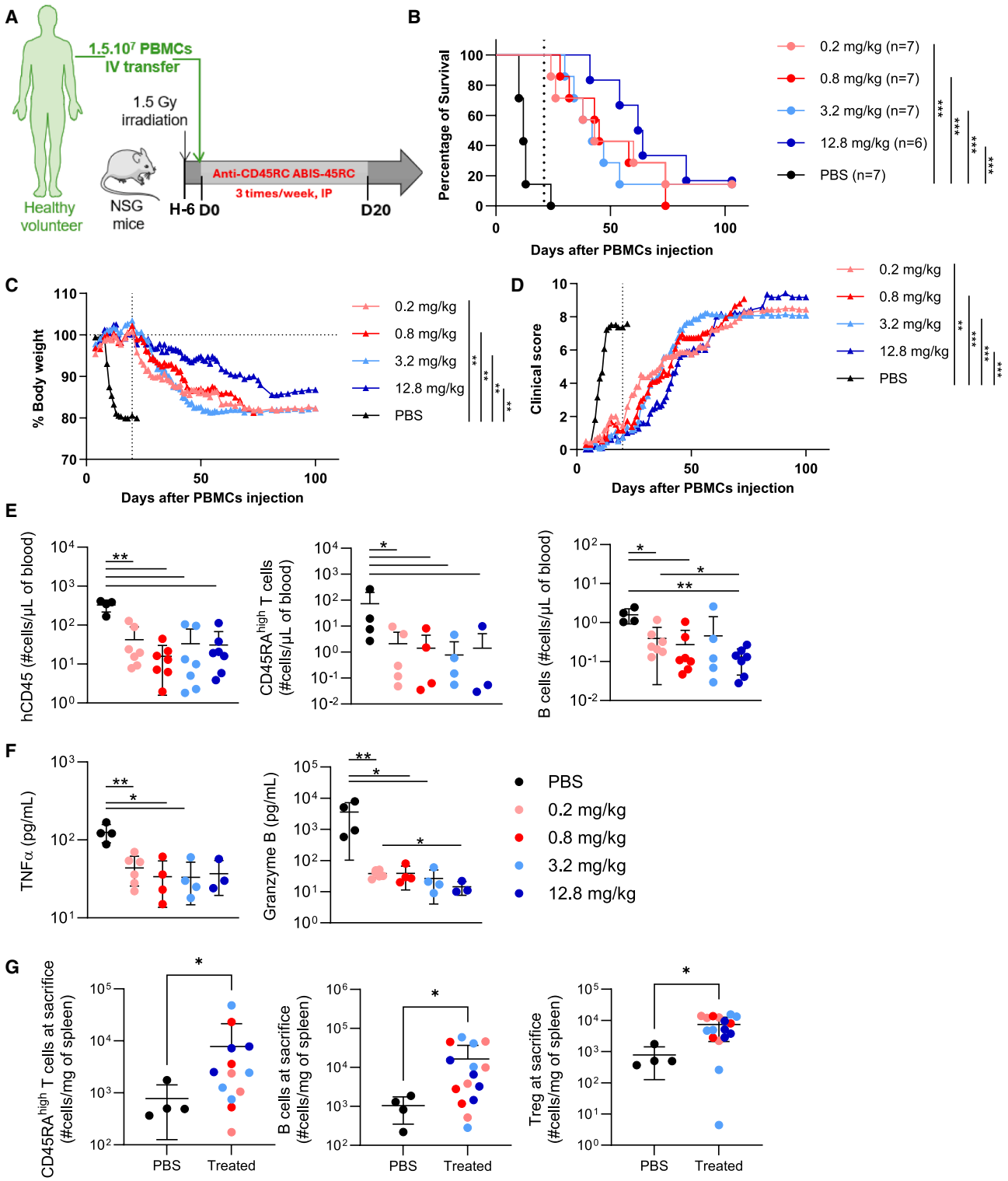

Figure 1. Chimeric anti-CD45RC mAb ABIS-45RC prevents acute GvHD in a humanized NSG mouse model

(A) Schematic of the protocol: 8-week-old NSG mice were irradiated with 1.5 Gy 6 h prior to IV injection of 1.5×10^7 human PBMCs (hPBMCs) from healthy volunteers. ABIS-45RC mAb was administered IP concomitant with PBMC injection for the first dose, followed by three injections per week for 3 weeks at 4 different doses: 12.8 mg/kg ($n = 6$),

(legend continued on next page)

conventional DCs, and plasma cells. Its restricted expression on pathogenic Th1 precursors, Th1 cells and TEMRA cells, sparing and absence on critical immune regulators like Treg cells, makes CD45RC a highly interesting target for therapeutic intervention.

Previous work, including ours, uncovered the absence of expression of CD45RC on FOXP3$^+$ CD4$^+$ and CD8$^+$ Treg cells underpinning clinical translation by means of cell therapy with CD8$^+$ CD45RC$^{low/neg}$ Treg cells in kidney transplant rejection.[9,11,13–15] Additionally, preclinical studies in animal models, including rat models of cardiac transplant rejection,[8] graft-versus-host disease (GvHD),[10] Duchenne muscular dystrophy,[16] and autoimmune polyendocrinopathy-candidiasis-ectodermal dystrophy (APECED),[17] demonstrated that an anti-CD45RC mAb effectively ameliorated and controlled these diseases. More specifically, these studies revealed that an anti-CD45RC mAb eliminates pathogenic T cells while preserving memory T and B cells, maintaining immune defense against pathogens. Importantly, the depletion of proliferating T and B cells promotes CD4$^+$ and CD8$^+$ Treg cell activation and proliferation, resulting in long-term tolerance. This effect persisted long after cessation of the treatment.

While promising, the mode of action (MoA) of anti-CD45RC mAbs on human immune cells has not been fully elucidated. Furthermore, prior studies utilized a murine immunoglobulin G1 (IgG1) OX22 clone with limited Fc effector functions, thus leaving the potential of fully competent mAb backbones with enhanced effector functions unexplored. The therapeutic efficacy of mAbs often depends on natural functions such as antigen blocking, signaling, pro-apoptotic activation, or engagement of effector pathways like antibody-dependent cell-mediated cytotoxicity (ADCC) upon binding of the mAb Fc fragment to the Fc gamma receptor (FcγR) of NK cells, complement-dependent cytotoxicity (CDC) involving killing by the complement cascade, and antibody-dependent cellular phagocytosis (ADCP) mediated by mAb Fc-fragment engagement of macrophages' FcγRs triggering engulfment of target cells.[18] A comprehensive understanding of the MoA is critical for optimizing dosing strategies and indication selection, while minimizing off-target effects.

To address these gaps, we characterized an anti-human CD45RC mAb with a humanized paratope and a human IgG1 Fc fragment capable of effector functions such as complement activation and FcγR binding. We evaluated its efficacy in a human acute GvHD (aGvHD) model using peripheral blood mononuclear cell (PBMC)-humanized immunodeficient mice, assessed its pharmacodynamic (PD) effects in CD34$^+$-humanized mice, and dissected its MoA in depleting CD45RC^{high} cells.

RESULTS

ABIS-45RC, a chimeric anti-human CD45RC IgG1 mAb, induces protection in a xenogeneic aGvHD model in humanized immunodeficient mice

To evaluate the therapeutic efficacy of ABIS-45RC, a chimeric anti-human CD45RC IgG1 mAb,[10] a dose-response study was conducted in a xenogeneic aGvHD model using immune-humanized immunodeficient NOD scid gamma (NSG) mice (Figure 1A). ABIS-45RC was administered as a monotherapy 3 times per week for 20 days, with doses of 0.2, 0.8, 3.2, and 12.8 mg/kg, covering a 100-fold dose range. This included a low total dose of approximately 0.036 μg to test the minimal efficacy threshold. Assessment of survival (Figure 1B), weight loss (Figure 1C), and clinical score (Figure 1D) demonstrated that all doses of anti-CD45RC mAb significantly delayed aGvHD compared to the phosphate-buffered saline (PBS) vehicle control group, in which all mice succumbed by day 21. Remarkably, long-term survival was observed in some mice across all dose groups, indicating efficacy even at the lowest dose of 0.2 mg/kg (0.036 μg total). No significant differences were observed among the dose groups, suggesting that the lowest dose was sufficient to delay aGvHD progression. Notably, signs of aGvHD only started to emerge after cessation of dosing on day 20 in all groups.

Blood analysis on day 14 revealed a significantly lower number of human CD45$^+$ (hCD45$^+$) cells in anti-CD45RC mAb-treated mice compared to the PBS control (Figure 1E, left), suggesting that ABIS-45RC effectively inhibits the proliferation of specific human PBMC (hPBMC) subsets activated in the aGvHD process. No dose-dependent differences in hCD45$^+$ cell numbers were observed among the different dose groups, reflecting the absence of significant differences in the survival curves. Given the absence of alternative anti-hCD45RC mAbs recognizing a different epitope for co-staining without steric hindrance, we used an anti-CD45RA mAb as a surrogate marker for CD45RC^{high} cells. The rationale for the surrogate marker is based on prior evidence demonstrating that most CD45RC^{high} cells also express CD45RA, except for FOXP3$^+$ Tregs, which are CD45RC^{neg} CD45RA^{high}.[8]

Analysis of blood CD45RA^{high} T and B cells at day 14 showed a reduction in their numbers in the blood of ABIS-45RC-treated mice compared to the PBS group, as expected, with no differences among doses (Figure 1E, center and right). Additionally, human serum cytokine analysis revealed significantly reduced levels of

3.2 mg/kg (n = 7), 0.8 mg/kg (n = 7), 0.02 mg/kg (n = 7), or PBS (n = 7). (B–D) Mice were monitored for (B) survival (assessed with a Mantel-Cox log rank statistical test; ***$p < 0.001$), (C) weight loss, and (D) mean clinical score (data shown as mean; assessed with a two-way ANOVA mixed-effect model with Geisser-Greenhouse correction; **$p < 0.005$; ***$p < 0.001$). (E and F) (E) Blood and (F) plasma samples were analyzed at day 14 to assess human CD45 expression, CD45RA^{high} T and B cells (blood, data presented as absolute count of cells per μL blood), and human cytokines (plasma) (*$p < 0.05$; **$p < 0.01$). (G) Spleens were collected at sacrifice to evaluate the presence of human CD45RA^{high} T cells, B cells, and Tregs (data presented as absolute count of cells per mg of spleen). Data are presented as mean (SD) and were assessed with a Mann-Whitney test (*$p < 0.05$). ANOVA, analysis of variance; GvHD, graft-versus-host disease, IP, intraperitoneal; IV, intravenous; mAb, monoclonal antibody; NSG, NOD scid gamma; PBMCs, peripheral blood mononuclear cells; PBS, phosphate-buffered saline; SD, standard deviation.

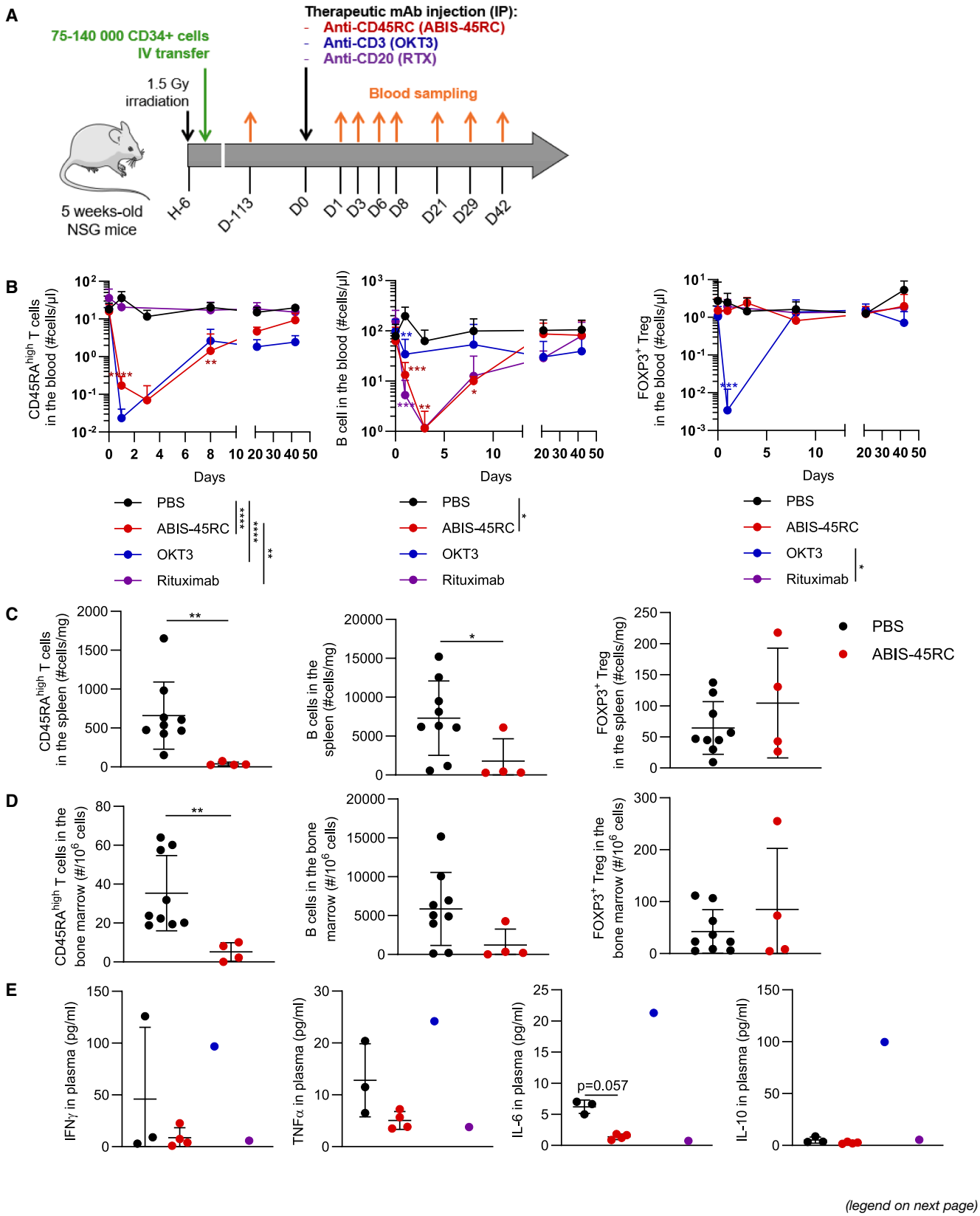

(legend on next page)

tumor necrosis factor α (TNF-α) and granzyme B in anti-CD45RC mAb-treated mice (Figure 1F), indicative of diminished inflammatory activity associated with an aGvHD. Levels of interleukin-10 (IL-10), IL-6, IL-2, and interferon-γ (IFN-γ) remained unchanged (data not shown).

Postmortem spleen analysis (conducted at the time of sacrifice between 4 and 83 days after the final dose) demonstrated a significant increase in the absolute number of FOXP3$^+$ Treg cells/mg of spleen in treated groups compared to the PBS control group (Figure 1G, right), as well as a recovery of CD45RA^{high} T and B cells (Figure 1G, center and left).

These findings demonstrate that ABIS-45RC effectively controls xenogeneic aGvHD in humanized mice during treatment, with efficacy observed even at a starting dose of 0.2 mg/kg. The results highlight its potential as a therapeutic drug to modulate immune responses in aGvHD.

Anti-CD45RC mAb efficacy is mediated by human CD45RC^{high} T and B cells depletion *in vivo*

To further evaluate the therapeutic effect of ABIS-45RC *in vivo*, we used immunodeficient NSG mice reconstituted with human CD34$^+$ cells, enabling the development of diverse human immune cell populations over 100–250 days post-reconstitution (Figure 2A). Mice with >60% hCD45$^+$ cells and >10% hCD3$^+$ cells on average (Figure S1A) were divided into groups and administered a single intraperitoneal (IP) dose of ABIS-45RC. These groups were compared to controls treated with anti-CD3 (clone OKT3) or anti-CD20 (rituximab [RTX]) mAbs, which selectively deplete T or B cells, respectively (Figure 2A). Of note, CD34$^+$ cells do not express CD45RC (Figure S1B).

By day 1 post-treatment, a significant depletion of CD45RA^{high} T cells was observed in the blood of mice treated with ABIS-45RC or anti-CD3 mAbs compared to PBS and anti-CD20-treated groups (Figure 2B, left). T cell levels returned to normal by day 40 post-treatment in mice treated with ABIS-45RC and anti-CD3 mAbs. For B cells, an almost complete depletion was observed by day 3 post-treatment in mice treated with either ABIS-45RC or anti-CD20 mAbs (Figure 2B, center). Recovery of B cells was slightly faster compared with T cells, with B cell levels normalizing by day 20 post-treatment. In contrast to the anti-CD3 mAb, which significantly depleted FOXP3$^+$ Treg cells, ABIS-45RC preserved this cell population (Figure 2B, right), corroborating findings in the aGvHD model (Figure 1G, right) and prior findings.[8,10,17] Additionally, ABIS-45RC caused only a partial and transient depletion of CD45RA^{low} T cells (day 1–day 3, normalized by day 8 post-treatment) and did not deplete CD45RA^{neg} T cells in the blood. In contrast, the anti-CD3 mAb almost completely depleted the CD45RA^{low} and CD45RA^{neg} T cell populations (Figure S1C).

At sacrifice (day 42 post-treatment), CD45RA^{high} T and B cells remained significantly depleted in the spleen and bone marrow of ABIS-45RC-treated mice compared to PBS controls (Figures 2C and 2D, left and center). As observed in blood, ABIS-45RC caused a partial depletion of CD45RA^{low} cells but not of CD45RA^{neg} T cells in the spleen and bone marrow (Figures S1D and S1E). A slight increase in FOXP3$^+$ Treg cells was observed in both the spleen and bone marrow of some ABIS-45RC-treated mice, although this trend was not statistically significant (Figures 2C and 2D, right).

Plasma human cytokine analysis was measured at day 3 post-injection to assess early immune activation. As expected, a control mouse treated with anti-CD3 mAbs (OKT3) displayed elevated levels of IFN-γ, IL-10 (both ∼100 pg/mL), as well as TNF-α and IL-6 (∼20 pg/mL), after subtraction of background levels.[19] In contrast, mice treated with ABIS-45RC, anti-CD20 mAbs, or PBS showed no significant cytokine increase (Figure 2E), indicating that ABIS-45RC does not activate CD45RC^{high} T cells during depletion, avoiding cytokine release, unlike the activation observed with OKT3.[19]

All of these *in vivo* findings demonstrate that ABIS-45RC controls immune responses by selectively depleting CD45RC^{high} T and B cells while sparing FOXP3$^+$ Treg cells and avoiding cytokine activation.

CD45RC^{high} target cells depletion mainly involves apoptosis induction enhanced by cross-linking and ADCP

To investigate the mechanisms mediating CD45RC^{high} T and B cell depletion, the ability of anti-CD45RC mAbs to induce cell death was tested *in vitro* using hPBMCs under various conditions: in the absence or presence of a secondary anti-IgG antibody for cross-linking (Figures 3A and 3B) or in the presence of NK cells to assess ADCC activity (Figures 3C and 3D). Additionally, we generated an afucosylated variant of the antibody (chimeric ABIS-45RC^{aF}, <1% fucose; Table S1) next to chimeric ABIS-45RC mAbs (approximately 90% fucose). The absence of fucose has been shown to enhance mAb Fc-mediated functions, particularly ADCC[20] (Figure 3). ADCP

Figure 2. Pharmacodynamic *in vivo* assessment of chimeric ABIS-45RC mAb in a CD34$^+$ humanized NSG mouse model

(A) Schematic of the protocol: 5-week-old NSG mice were irradiated (1.5 Gy X-ray) 6 h prior to IV injection with 75,000–140,000 human CD34$^+$ cord blood cells. After 120–150 days, mice confirmed to be engrafted with B and T cells were injected IP with 0.8 mg/kg ABIS-45RC mAb (n = 10) compared to anti-CD3 (OKT3, n = 7) or anti-CD20 (rituximab [RTX], n = 7) mAbs as positive controls or PBS as negative control (n = 9). (B–D) (B) Blood (kinetics, data presented as absolute count of cells per μL blood), (C) spleen (data presented as absolute count of cells per mg of spleen), and (D) bone marrow (data presented as absolute count of cells per 10^6 harvested cells) samples (day 3) were analyzed by flow cytometry for CD45RA^{high} T and B cells or Tregs. (E) Human cytokines (IFN-γ, TNF-α, IL-6, and IL-10) were measured at day 3 in plasma using Ella. Data are presented as mean (SD) of two independent experiments and were assessed with a two-way ANOVA with Sidak's multiple comparison test for blood samples and a Mann-Whitney test for spleen, bone marrow, and plasma samples (*p < 0.05; **p < 0.01; ***p < 0.001; ****p < 0.0001). IFN-γ, interferon-γ; IL, interleukin; TNF-α, tumor necrosis factor-α.

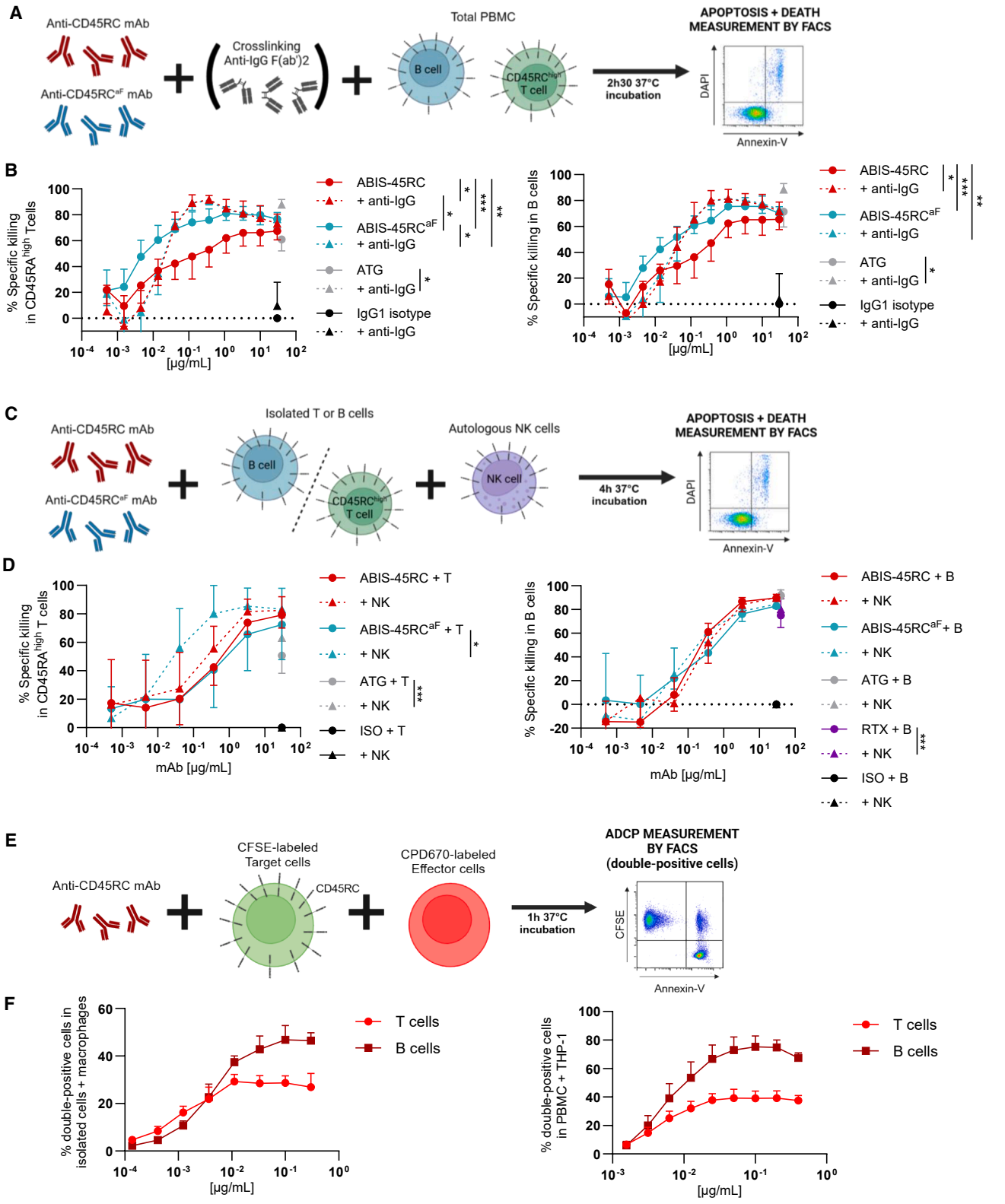

(legend on next page)

activity was also assessed with isolated T and B cells or PBMCs in the presence of monocyte-derived macrophages or monocytic cell line THP-1 (Figures 3E and 3F).

In vitro, ABIS-45RC induced the dose-dependent cell death of CD45RA^{high} T and B cells among PBMCs, as measured by specific killing (readout taking into account apoptosis, as well as lysis, normalized on isotype condition). The 50% effective concentration (EC_{50}) values were 0.030 μg/mL for CD45RA^{high} T cells and 0.125 μg/mL for B cells, indicating greater sensitivity of T cells to the antibody (solid red lines, Figure 3B; Table 1). Cross-linking with a secondary F(ab)′2 antibody significantly enhanced this effect, lowering EC_{50} values to 0.017 μg/mL for CD45RA^{high} T and 0.033 μg/mL for B cells (dotted red lines, Figure 3B). The afucosylated ABIS-45RC^{aF} mAb demonstrated significantly higher killing efficiency compared to ABIS-45RC, with EC_{50} values of 0.004 μg/mL for CD45RA^{high} T cells and 0.021 μg/mL for B cells in the absence of secondary IgG (solid blue line, Figure 3B). However, cross-linking slightly reduced the killing efficiency of afucosylated mAb, resulting in EC_{50} values of 0.016 μg/mL for CD45RA^{high} T cells and 0.033 μg/mL for B cells (dotted blue line, Figure 3B; Table 1). This suggests that for the afucosylated mAb cross-linking with antibodies may interfere with Fc-mediated mechanisms by FcγR^{+} cells in PBMCs, such as monocytes and NK cells, by masking FcγR interactions.

The cross-linking antibody, added at a fixed concentration, enhanced apoptosis-induced cytotoxicity within a specific dose range, suggesting a ratio-dependent effect between anti-CD45RC and crosslinking antibodies. Notably, although no specific killing was observed for CD45RA^{neg} T cells, the presence of the cross-linking antibody induced cytotoxicity in CD45RA^{low} T cells at a concentration of around 0.37 μg/mL of anti-CD45RC mAb, suggesting that crosslinking lowers the density threshold required for anti-CD45RC mAb induced cytotoxicity (Figure S2A).

To confirm the role of Fc-mediated mechanisms, we performed an ADCC assay using NK cells as effectors in the presence of isolated T or B cells from PBMCs and either ABIS-45RC or afucosylated ABIS-45RC^{aF} mAbs (Figures 3C and 3D; Table 1). While ABIS-45RC showed no significant ADCC activity in this context, the afucosylated ABIS-45RC^{aF} mAb induced significant CD45RA^{high} T but not B increased cell death *in vitro* in the presence of NK cells. While no dose-response curves were generated for the reference antibodies RTX and anti-thymoglobulin (ATG), the enhanced *in vitro* depletion observed with ABIS-45RC at equivalent concentrations underscores its potent activity and supports its potential as an effective dual-targeting immunotherapy. No specific killing of CD45RA^{low} or CD45RA^{neg} T cells was observed with either mAb, contrasting with the broad activity of antibodies (Figure S2B).

We also assessed the role of CDC in cell lysis and found that anti-CD45RC mAb failed *in vitro* to induce killing of CD45RA^{high} T and B cells in the presence of complement (Figure S3). This effect is likely attributable to the considerable length of the CD45RABC molecule, with antibody binding occurring at its distal end, as both CDC and ADCC efficiency decrease with increasing distance from the cell membrane.[21]

Finally, we evaluated the potential of the anti-CD45RC mAb to mediate ADCP (Figures 3E and 3F; Table 1). In the presence of isolated blood CD45RC^{high} T and B cells and monocyte-derived macrophages, the anti-CD45RC mAb induced dose-dependent ADCP, with EC_{50} values of 0.001 μg/mL for CD45RC^{high} T and 0.004 μg/mL for B cells (Figure 3F, left). Similar dose-dependent ADCP activity was observed with total PBMCs and the monocytic THP-1 cell line, yielding EC_{50} values of 0.005 μg/mL for CD45RC^{high} T and 0.007 μg/mL for B cells (Figure 3F, right). It has been noted that ADCP efficiency augments with increased distance between the epitope recognized by an antibody and the cell membrane.[21]

These results demonstrate that anti-CD45RC mAb induces target cell death primarily through intrinsic cell signaling through CD45RC, which is increased by cross-linking, and ADCP.

Cell membrane density and high-affinity binding of CD45RC are critical for anti-CD45RC mAb-induced cell death

To confirm isoform specificity, human embryonic kidney (HEK) 293T cell lines were transduced with lentiviral vectors encoding for

Figure 3. Chimeric ABIS-45RC mAb triggers apoptosis-induced cytotoxicity enhanced through crosslinking and demonstrates ADCP activity

(A) Schematic of the cytotoxicity experiment setup. (B) hPBMCs were treated for 2.5 h with a dose range of ABIS-45RC (red, $n = 4$) or afucosylated ABIS-45RC^{aF} (blue, $n = 4$), or with a single dose of ATG (gray, $n = 4$) or isotype control mAb (black, $n = 4$) as positive or negative controls, respectively, in the presence or absence of a secondary anti-IgG F(ab′)2 crosslinking antibody (plain vs. dotted lines). Specific killing was analyzed by flow cytometry using annexin V and DAPI staining. Data are presented as mean (SD) of three independent experiments and were assessed with a two-way ANOVA with Sidak's multiple comparison test for anti-CD45RC mAb conditions (*$p < 0.05$; **$p < 0.01$; ***$p < 0.001$) and a Mann-Whitney test for ATG and isotype control comparisons (*$p < 0.05$). (C) Schematic of the ADCC experiment setup. (D) Isolated T cells ($n = 7$, left) or B cells ($n = 4$, right) were co-cultured for 4 h with (dotted lines) or without (solid lines) autologous NK cells in the presence of a dose range of ABIS-45RC (red) or afucosylated ABIS-45RC^{aF} (blue) mAbs or ATG or RTX as positive controls and isotype as the negative control. Specific killing was measured by flow cytometry using annexin V and DAPI staining. Data are presented as mean (SD) of at least two independent experiments, and statistical differences were assessed with a two-way ANOVA with Sidak's multiple comparison test for the upper images and a Mann-Whitney test for the lower images (*$p < 0.05$; ***$p < 0.001$). (E) Schematic of the ADCP experiment setup. (F) Isolated T or B cells (CFSE labeled, $n = 4$, left) were co-cultured for 1 h with monocyte-derived macrophages (CPD670-labeled, left) or hPBMCs (CFSE labeled) with the THP-1 monocytic cell line (CPD670 labeled, right), in the presence of a dose range of ABIS-45RC. ADCP was measured by flow cytometry as the percentage of double-positive CPD670- and CFSE-labeled cells. Data are presented as mean (SD). ADCP, antibody-dependent cellular phagocytosis; ATG, anti-thymocyte globulin; ABIS-45RC^{aF}, afucosylated chimeric anti-CD45RC mAb; CFSE, carboxyfluorescein succinimidyl ester; CPD670, cell proliferation dye 670 nm; DAPI, 4′,6-diamidino-2-phenylindole; IgG, immunoglobulin G; NK, natural killer.

Table 1. EC_{50} data obtained from chimeric ABIS-45RC and humanized ABO21009 anti-CD45RC mAbs induced binding, cytotoxicity through direct apoptosis, ADCC, and ADCP

Direct cytotoxicity ± crosslinking antibody (% specific killing)				
	Without crosslinking antibody		With crosslinking antibody	
	ABIS-45RC	ABIS-45RC^{aF}	ABIS-45RC	ABIS-45RC^{aF}
CD45RA^{high} T cells	0.030 (0.019)	0.004 (0.002)	0.017 (0.007)	0.016 (0.002)
B cells	0.125 (0.117)	0.021 (0.027)	0.033 (0.023)	0.033 (0.020)
Cytotoxicity by ADCC on isolated T and B cells (% specific killing)				
	Without NK cells		With NK cells	
	ABIS-45RC	ABIS-45RC^{aF}	ABIS-45RC	ABIS-45RC^{aF}
CD45RA^{high} T cells	0.53 (0.21)	0.86 (0.79)	0.26 (0.15)	0.03 (0.04)
B cells	0.16 (0.08)	0.36 (0.09)	0.34 (0.16)	0.10 (0.08)
ADCP on T and B cells (% DP)				
	PBMCs + macrophages		PBMCs/cell line + THP-1	
T cells	0.001 (0.000)		0.005 (0.001)	
B cells	0.004 (0.001)		0.007 (0.002)	
ELISA (OD_{450})				
	ABIS-45RC		ABO21009	
CD45RABC	0.043 (0.009)		0.047 (0.014)	
FACS (% CD45RC^{high+} cells)				
	ABIS-45RC		ABO21009	
CD45RA^{high} T cells	0.18 (0.07)		0.23 (0.06)	
B cells	0.28 (0.01)		0.38 (0.10)	
Direct cytotoxicity by ABO21009 ± crosslinking antibody (% specific killing)				
	Without crosslinking antibody		With crosslinking antibody	
CD45RA^{high} T cells	0.054 (0.047)		0.032 (0.15)	
B cells	0.127 (0.086)		0.060 (0.019)	
ADCP by ABO21009 on T and B cells (% DP)				
	PBMCs + macrophages		PBMCs/cell line + THP-1	
T cells	0.019 (0.005)		0.011 (0.001)	
B cells	0.023 (0.007)		0.017 (0.005)	
Daudi	NA		0.030 (0.003)	
MOLT-4^{RC}	NA		0.040 (0.011)	

EC_{50} was calculated through four-parameter sigmoid regression analysis of curves obtained with raw data (% specific killing, % DP, OD_{450}). Data are presented as mean (SD). ADCC, antibody-dependent cellular cytotoxicity; ADCP, antibody-dependent cellular phagocytosis; DP, double-positive cells; EC_{50}, effective concentration 50%; ELISA, enzyme-linked immunosorbent assay; FACS, fluorescence-activated cell sorting; mAb, monoclonal antibody; NA, not applicable; NK, natural killer; OD, optical density; PBMCs, peripheral blood mononuclear cells; SD, standard deviation.

human CD45RA, CD45RB, CD45RC, CD45RO, or CD45RABC isoforms (Figure 4A). The anti-CD45RC mAb exclusively recognized the C domain of the CD45RC and CD45RABC isoforms, with no detectable cross-reactivity with other CD45 isoforms, further validating its specificity.

To understand the mechanism of anti-CD45RC mAb-induced cell death, we quantified the surface density of CD45RC molecules across T and B cell subsets. Using a phycoerythrin (PE)-labeled anti-CD45RC mAb calibrated against PE-coated reference beads, we calculated the density of CD45RC molecules per μm^2 and total molecules per cell, incorporating cellular volume estimates obtained with size-calibrated beads (Figures 4B and S4A; Table S2). CD45RC^{high} T cells exhibited a higher density than B cells with, respectively, 31 and 24 molecules/μm^2 of membrane corresponding to approximately 24,000 molecules per T cell and 17,000 molecules per B cell. CD45RC^{low} T cells expressed fewer than 2 molecules/μm^2 of membrane, and as expected, CD45RC expression was undetectable in T cells identified in the CD45RC^{neg} gate.

Using ELISA, we measured the affinity of ABIS-45RC binding to the recombinant human CD45RABC (rhCD45RABC) protein and

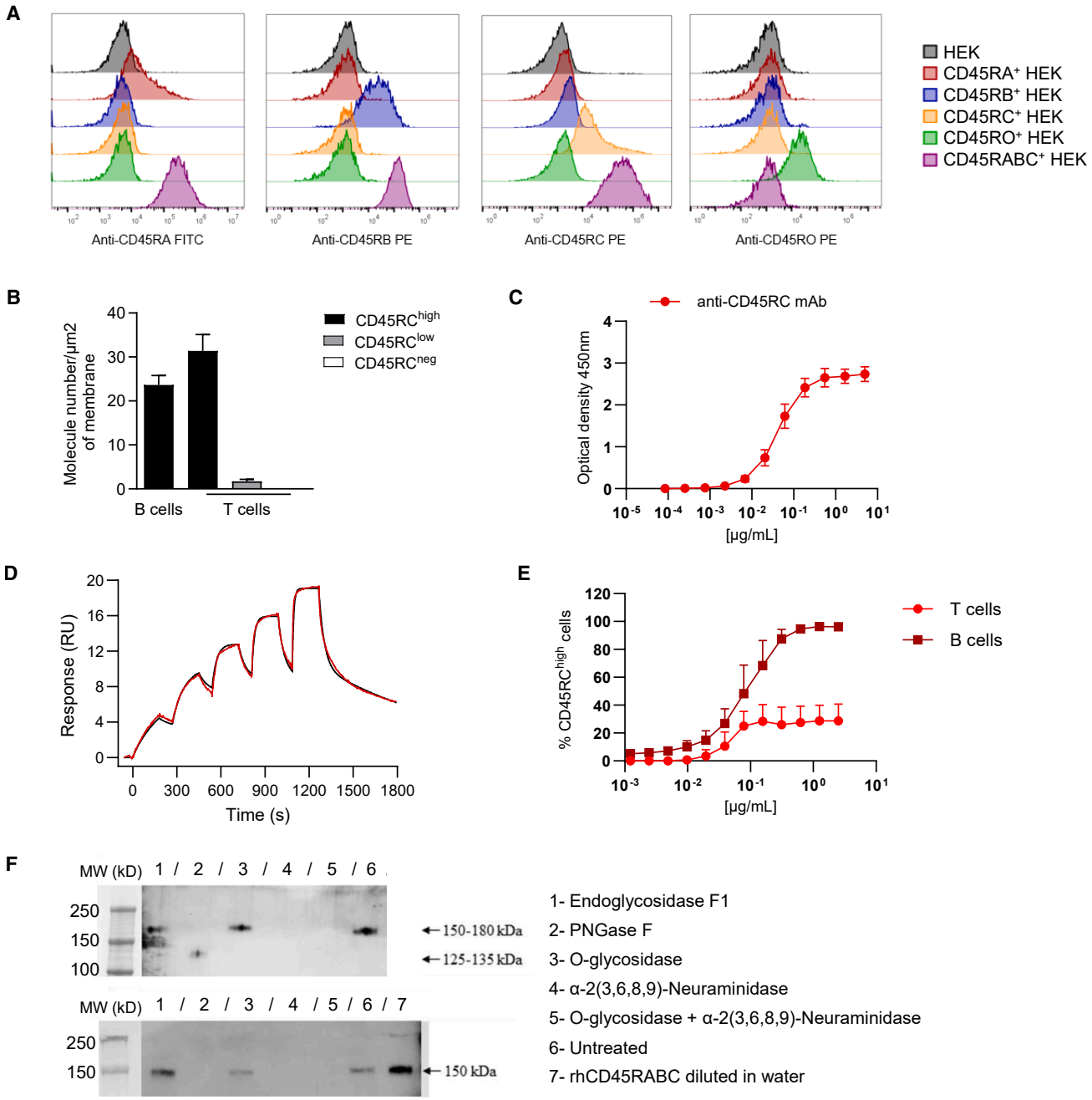

Figure 4. Quantification and binding specificity of anti-CD45RC mAb

(A) Specificity of ABIS-45RC mAb was assessed on HEK cells transduced with CD45RA, -RB, -RC, -RO or -RABC isoforms. Transduced cells were probed with isoform-specific antibodies (anti-RA, -RB, or -RO) and ABIS-45RC. Data are representative of two independent experiments. (B) Quantification of CD45RC molecules on fresh hPBMCs, expressed as the total number of CD45RC molecules per μm^2 of membrane. B and T cells were analyzed and subdivided in $CD45RC^{high}$ (black bar), $CD45RC^{low}$ (gray bar), and $CD45RC^{neg}$ (white bar) populations when appropriate (n = 9). Data are presented as mean (SD) of three independent experiments. (C) Recognition of recombinant CD45RABC protein by ABIS-45RC measured at an optical density of 450 nm by ELISA (n = 6). Data are presented as mean (SD) of six independent experiments. (D) Single-cycle kinetic interaction analysis of ABIS-45RC mAb at concentrations of 3.7, 11.1, 33.3, 100, and 300 nM with captured CD45RABC using SPR (Biacore). (E) Percentage of T or B cells in the $CD45RA^{high}$ gate stained with a dose range of ABIS-45RC mAb and a secondary fluorescent anti-human IgG, measured by flow cytometry

(legend continued on next page)

determined an EC_{50} of 0.043 μg/mL (Figure 4C). Binding kinetics and affinity analyses of the anti-CD45RC mAb to rhCD45RC protein produced in eukaryotic cells to include glycosylation was performed using Biacore and demonstrated an association rate of 8.34×10^5 M^{-1} s^{-1}, a dissociation rate of 9.67×10^{-4} s^{-1}, and an equilibrium binding constant affinity (K_D) of 1.16 nM (Figure 4D; Table S3). The relative affinity of the anti-CD45RC mAb by flow cytometry of $CD45RC^{high}$ T and B cells revealed EC_{50} values of 0.18 and 0.28 μg/mL, respectively (Figure 4E; Table 1). These values highlight the high-affinity binding of the mAb across cell types.

To elucidate the molecular basis of ABIS-45RC recognition, we analyzed binding to rhCD45RABC protein under denaturing (Figure 4F, top) and native (Figure 4F, bottom) conditions, as well as following enzymatic deglycosylation. ABIS-45RC bound untreated rhCD45RABC under both denaturing and native conditions (lanes 6–7, respectively), while enzymatic treatments revealed critical roles for specific glycans. N-linked glycans and sialic acid residues were required for recognition since binding was abrogated by PNGaseF (lane 2), which removes all asparagine-linked complexes, hybrids, or high mannose oligosaccharides, and by α-2(3,6,8,9)-neuraminidase (lanes 4 and 5), which cleaves linear and branched terminal sialic acid residues. Removal of O-glycans alone did not affect the binding of ABIS-45RC (lane 3), nor did endoglycosidase F1 (lane 1), which specifically cleaves N-linked oligosaccharides between the two N-acetylglucosamine residues in the diacetylchitobiose core of the oligosaccharide. Given that sialic acid is present in human serum and plasma at concentrations around 0.2 μg/mL and can increase under certain clinical conditions,[22] we evaluated its effect in a binding assay and found that the addition of sialic acid, in the presence or absence of human plasma, did not interfere with the mAb binding in contrast to the addition of soluble rhCD45RABC as a positive control (Figure S4B). These findings indicate that amino acids, N-linked glycans, and sialic acid residues collectively contribute to the epitope recognized by the anti-CD45RC mAb.

These results show that the anti-CD45RC binds specifically to $CD45RC^{high}$ subsets of T and B cells, with no cross-reactivity to other CD45 isoforms. High surface density of CD45RC molecules correlates with susceptibility to mAb-induced cell death. The linear epitope recognized by the mAb involves a complex interplay of N-glycans, sialic acids, and amino acid residues.

ABO21009, a humanized anti-CD45RC mAb, demonstrates direct apoptosis-induced cytotoxicity and ADCP as its key mechanisms of action

ABO21009, a humanized IgG1 therapeutic drug candidate derived from the chimeric ABIS-45RC mAb, was selected and fully characterized. ABO21009 efficiently and specifically bound CD45RC and induced dose-dependent specific killing of $CD45RA^{high}$ T and B cells among PBMCs (Figures 5A and S5A; Tables 1 and S3). The addition of NK cells did not significantly enhance specific killing of $CD45RA^{high}$ T and B cells (Figure S5B), and activation of NK cells, assessed by CD107a expression, occurred only with the afucosylated variant of ABIS-45RC (Figure 5B). In contrast, the evaluation of ADCP demonstrated significant dose-dependent phagocytosis of isolated T and B cells by monocyte-derived macrophages (Figure 5C, left) and total PBMCs by the THP-1 monocytic cell line (Figure 5C, right), highlighting the prominent role of ADCP in the mechanism of action of ABO21009 (Table 1). We did not observe killing of $CD45RA^{high}$ T and B cells in the presence of rabbit (Figure S5C) or human complement (Figure S5D). In the same manner as ABIS-45RC, ABO21009 did not trigger any cytotoxicity in $CD45RC^{low}$ or $CD45RC^{neg}$ T cells (Figure S5).

The binding of ABO21009 to FcγRs and the neonatal Fc receptor (FcRn) was evaluated to assess its compatibility with established Fc-mediated mechanisms.[23] The results confirmed that ABO21009 exhibits binding profiles in line with the expected behavior of a human IgG1 backbone, ensuring efficient interaction with FcγRs involved in effector functions such as ADCP (Table S4). Additionally, ABO21009 demonstrated binding to FcRn with values of 5.43×10^{-7} M, similar to commercial trastuzumab with values of 5.39×10^{-7} M, in a pH-dependent manner, supporting its potential for extended serum half-life and efficient recycling.

Analysis of various cell lines revealed that the Daudi B cell line was uniformly 100% positive for CD45RC, whereas tested T cell lines, including Human T cell-78, Jurkat, Minneapolis Line of T cells 4 (MOLT-4) and Children's Cancer Research Foundation-CEM, lacked CD45RC expression (Figure 5D) (data not shown). To overcome this limitation, we generated a CD45RC-expressing T cell line by transducing the MOLT-4 cell line with a lentiviral vector encoding CD45RABC (Figure 5D, right). The resulting $MOLT\text{-}4^{RC}$ cell line expressed comparable numbers of CD45RC molecules per cell to $CD45RC^{high}$ T and B cells and the Daudi cell line (Figure S6). However, both Daudi and $MOLT\text{-}4^{RC}$ cells exhibited a lower CD45RC density per μm^2 of membrane due to their larger cell size compared to primary $CD45RC^{high}$ lymphocytes (Figure 5E).

The ability of ABO21009 to induce ADCP using THP-1 cells as an effector was assessed and a dose-dependent increase in phagocytosis was observed in Daudi and $MOLT\text{-}4^{RC}$ cell lines, with EC_{50} values of 0.03 and 0.04 μg/mL, respectively (Figure 5F; Table 1). To confirm that this assay was reminiscent of true phagocytosis, confocal microscopy with carboxyfluorescein succinimidyl ester (CFSE)-labeled Daudi cells (green) and CDP670-labeled monocyte-derived macrophages (purple) was performed (Figure 5G). Analysis revealed a

(*n* = 8). Data are presented as mean (SD) of eight independent experiments. (F) Western blot analysis using ABIS-45RC mAb for the detection of CD45RABC protein after deglycosylation treatments under denaturing/reducing (top) and native (bottom) conditions. Treatments are listed as 17 in the key at right. Arrows indicate protein bands. ELISA, enzyme-linked immunosorbent assay; HEK, human embryonic kidney; MW, molecular weight; PNGase F, peptide:*N*-glycosidase F; rhCD45RABC, recombinant human CD45RABC; SPR, surface plasmon resonance.

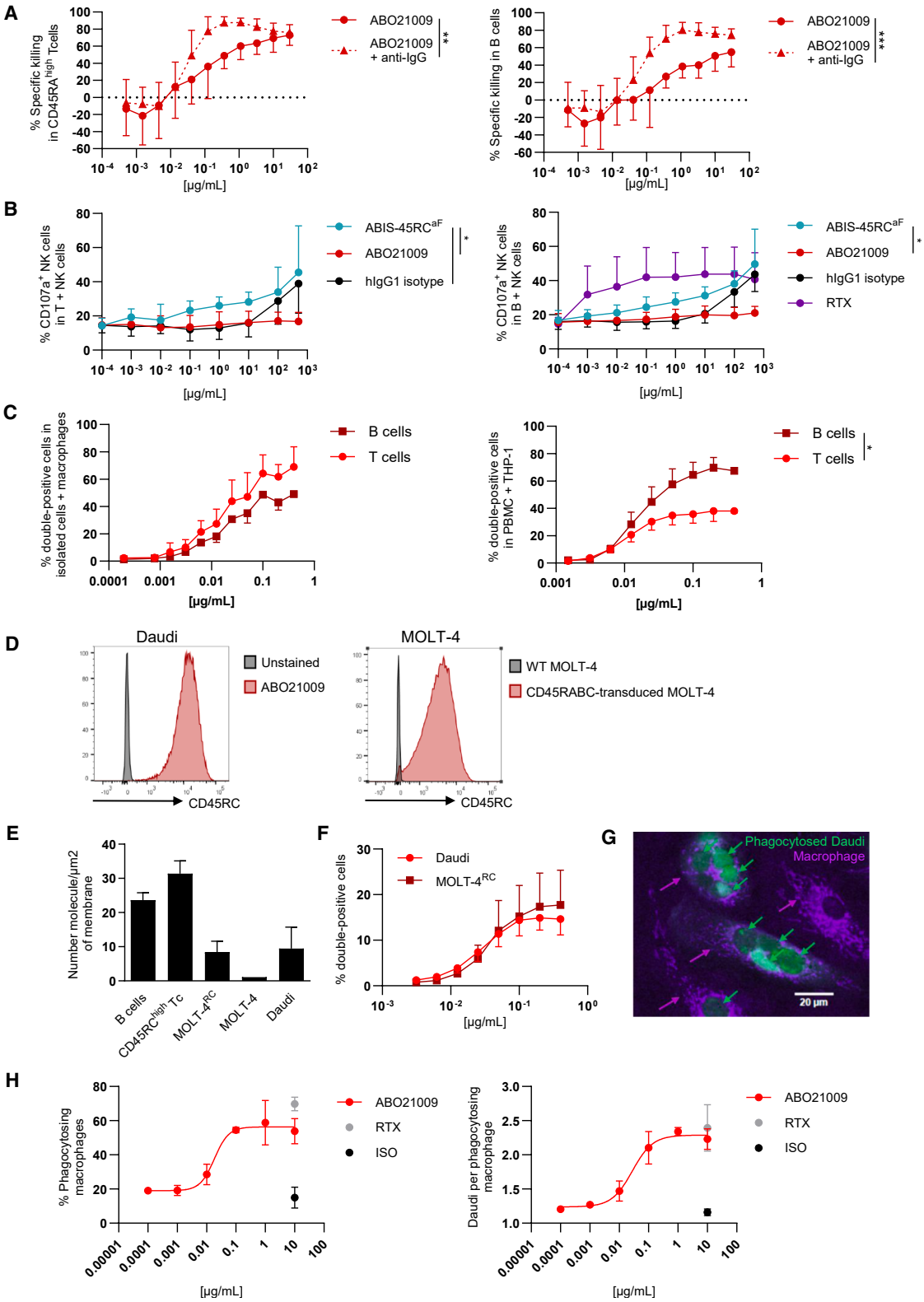

(legend on next page)

plateau at 1 μg/mL, where around 60% of macrophages were actively phagocytosing, with an average of 2 Daudi cells phagocytosed per macrophage, comparable to the effect observed with RTX (Figure 5H). Although confocal microscopy showed that THP-1 cells are not able to phagocytose target Daudi cells (data not shown), the ADCP assay was reminiscent of true phagocytosis as EC_{50} of both assays were in the same range with EC_{50}s for the microscopy assay of 0.018 and 0.028 μg/mL for the percentage of phagocytosing macrophages and the number of Daudi cells per phagocytosing macrophage readouts.

These results demonstrate that ABO21009 efficiently induces ADCP as well as direct cytotoxicity, the primary mechanisms of action, with potent phagocytosis observed across multiple *in vitro* assays. The development of a robust ADCP assay using CD45RC-expressing cell lines highlights the therapeutic potential of ABO21009' for selectively targeting CD45RC^{high} cells.

In vivo evaluation of ABO21009 in immune system-humanized mice highlights its potential as a therapeutic candidate

We next assessed the *in vivo* efficacy of ABO21009 in a dose-dependent manner using the xenogeneic aGvHD model. A range of ABO21009 doses was selected starting from the previously defined minimal effective concentration for ABIS-45RC (Figure 1). Mice were treated with ABO21009 alone, 3 times per week for 20 days, to assess its efficacy in delaying aGvHD onset (Figure 6A). Survival rates and clinical scores revealed that doses of 0.2 and 0.8 mg/kg significantly delayed aGvHD progression compared with the PBS group. In contrast, lower doses of 0.0125 and 0.05 mg/kg failed to delay aGvHD (Figures 6B and 6D), suggesting that 0.2 mg/kg is the minimal effective dose in this model. Analysis of blood cells at day 15 confirmed a dose-dependent significant depletion of CD45RA^{high} T and B cells, correlating with therapeutic efficacy (Figure 6C).

To further understand the PD effects of ABO21009 in a model mimicking the human system, we tested two doses in CD34^{+} humanized NSG mice, 0.05 and 1 mg/kg, known to be, respectively, effective and ineffective in aGvHD animal models (Figures 6E and S7). Interestingly, both doses led to a rapid and significant depletion of CD45RA^{high} T cells within hours after administration of a single intravenous (IV) administration, reaching significant depletion for both doses (Figure 6F, left). The effect was more pronounced at the dose of 1 mg/kg. At the highest dose, ABO21009 also caused a partial depletion of CD45RA^{low} T cells normalized by day 40 post-treatment, and did not deplete CD45RA^{neg} T cells in the blood (Figure S7). B cells were significantly depleted only with the higher dose of 1 mg/kg and recovered quickly by day 16 post-treatment (Figure 6F, right). After administration of 0.05 mg/kg, CD45RA^{high} T cells fully recovered by day 8 post-treatment, whereas at 1 mg/kg, T cells recovered by day 44 post-treatment, underscoring the more prolonged depletion compared to B cells (recovery by day 20).

These results demonstrate that the duration of CD45RA^{high} T and B cells depletion correlates with the PD effect of ABO21009. The minimal effective dose of 0.2 mg/kg in the aGvHD model and the rapid but dose-dependent recovery of target cells in the humanized NSG model highlight the therapeutic potential of ABO21009 for precise immune modulation.

Single-cell transcriptome analysis of blood cells incubated with ABO21009 mAb *in vitro*

Finally, to comprehensively evaluate the impact of ABO21009 on total blood cells, we conducted single-cell RNA sequencing with cellular indexing of transcriptomes and epitopes sequencing (CITE-seq) using an anti-CD45RA antibody to track cell subsets. Blood samples from 3 healthy donors were incubated for 5 h with ABO21009 or an isotype control mAb (Figure 7A). In parallel, a cytotoxicity assay confirmed the depleting efficacy of ABO21009 on target cells (data not shown).

A total of 67,806 single cells, evenly distributed among the donors, met the inclusion criteria and were further processed (Figure S8A).

Figure 5. Humanized anti-CD45RC mAb ABO21009 triggers apoptosis-induced cytotoxicity and ADCP in CD45RC-expressing cells, enhanced by crosslinking

(A) Total hPBMCs ($n = 6$) were treated for 2.5 h with a dose range of humanized anti-CD45RC mAb (ABO21009) in the presence or absence of a secondary anti-IgG F(ab')2 crosslinking antibody (plain vs. dotted lines). Specific killing was analyzed by flow cytometry using annexin V and DAPI staining. Data are presented as mean (SD) and were assessed with a two-way ANOVA with Sidak's multiple comparison test between anti-CD45RC mAb conditions (**$p < 0.01$; ***$p < 0.001$). (B) NK cell activation was evaluated using CD107a expression by flow cytometry at a 5:1 effector-to-target (E:T) ratio, in the presence of T cells ($n = 5$) and B cells ($n = 4$). Data are presented as mean (SD) of at least two independent experiments and were assessed with a two-way ANOVA with Sidak's multiple comparison test (*$p < 0.05$). (C) For ADCP analysis, isolated T or B cells ($n = 4$) were co-cultured for 1 h with monocyte-derived macrophages, or hPBMCs with the THP-1 monocytic cell line, in the presence of a dose range of ABO21009. ADCP was analyzed by flow cytometry by measuring the percentage of double-positive cells. Data are provided as mean (SD) of at least two independent experiments and were assessed with a two-way ANOVA statistical test with Sidak's multiple comparison test. (D) Flow cytometry analysis of CD45RC expression on Daudi as well as WT and CD45RC-transduced MOLT-4 (MOLT-4^{RC}) cell lines. (E) Quantification of CD45RC molecule density (molecules/μm^2) of cell membrane, mean (SD) on WT or MOLT-4^{RC} cells, versus B and T cells (Tc) from fresh PBMCs. (F) Daudi ($n = 4$) or MOLT-4^{RC} ($n = 3$) were co-cultured for 1 h with THP-1 cells in the presence of a dose range of ABO21009, and ADCP was analyzed by flow cytometry (% DP cells). Data are provided as mean (SD) of at least three independent experiments. (G) CFSE-labeled Daudi cells were co-cultured for 1 h with CPD-670-labeled monocyte-derived macrophages in the presence of a dose range of ABO21009 (10–0.01 μg/mL, $n = 3$ in duplicate), RTX (positive control), or isotype (ISO, negative control) at 10 μg/mL. Confocal fluorescence microscope images show CFSE-labeled Daudi cells (green arrows) phagocytosed by CPD-670-labeled monocyte-derived macrophages (purple arrows). (H) Quantification of the percentage of phagocytosing macrophages and the number of Daudi cells phagocytosed per macrophage was performed using fluorescence microscope on double-labeled images. Data are presented as mean (SD) of duplicates of three independent experiments. CPD670, cell proliferation dye 670 nm; % DP, percentage of double-positive cells; WT, wild type.

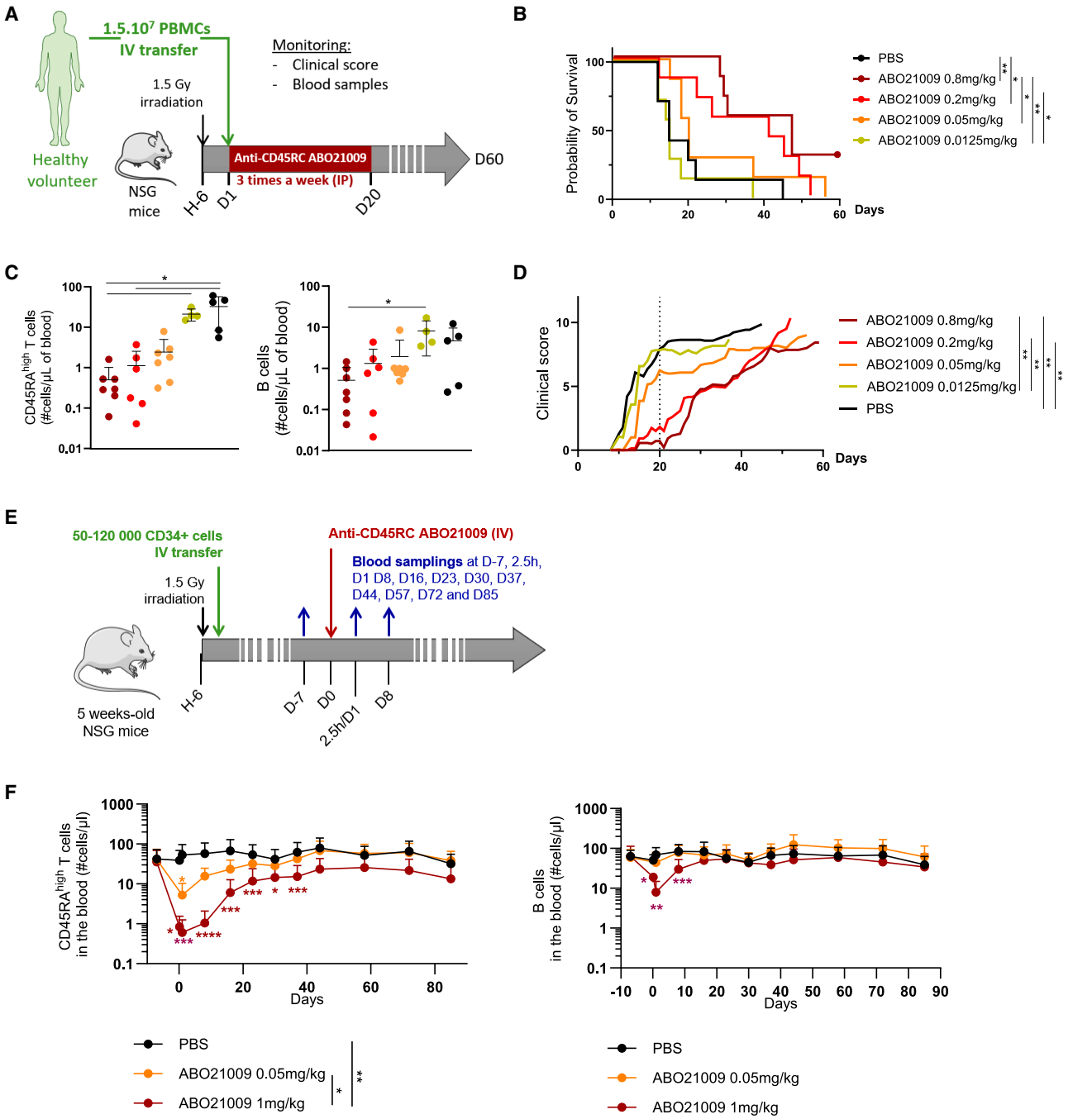

Figure 6. Humanized anti-CD45RC mAb ABO21009 prevents acute GvHD and depletes CD45RC^{high} cells in humanized NSG mouse models

(A) Schematic of the protocol: 8-week-old NSG mice (n = 7 per group) were irradiated with 1.5 Gy 6 h before IV injection of 1.5 × 10^7 hPBMCs from healthy volunteers. ABO21009 mAb was administered IP at varying doses, starting concomitantly with hPBMC injection and continuing three times weekly for 3 weeks. (B) Mice were monitored for survival, and data were assessed using a Mantel-Cox log rank test (*$p < 0.05$; **$p < 0.01$). (C) Blood samples were collected at day 15 to assess CD45RC^{high} T and B cells by flow cytometry (data presented as absolute count of cells per µL blood). Data are presented as mean (SD) and were assessed with a Mann-Whitney test (*$p < 0.05$). (D) Clinical scores were monitored over time. Data are presented as mean and were assessed with a two-way ANOVA with Sidak's multiple comparison test (**$p < 0.001$).

(legend continued on next page)

Data were integrated using Seurat, log-normalized and visualized by uniform manifold approximation and projection (UMAP). Quality controls, including read count and mitochondrial genes content, confirmed no major bias across samples.

Analysis of the CD45RA subsets using CITE-seq revealed a significant decrease in CD45RA^{high} cells following ABO21009 treatment compared to the isotype control, while CD45RA^{low} and CD45RA^{neg} populations remained unaffected (Figures 7B and S8B), demonstrating effective depletion of the target CD45RA^{high} subset without altering the broader T cell landscape.

To further delineate the effects, we applied an unsupervised analysis approach, performed dimensionality reduction using UMAP, and identified cell populations based on marker expression: CD14 for monocytes; CD3ε, CD4, and CD8α for T cell populations; KLRC1 for NK cells; and CD19 and CD22 for B cells (Figure 7C). Comparative analysis between isotype and ABO21009-treated samples showed reductions in CD45RA^{high} subsets within T and B cells, and a more pronounced depletion among T cells (Figure 7D).

Further subset analysis of 10153 CD45RA^{high} T cells (Figure 7E) and 6496 B cells (Figure 7F) confirmed the depletion of most CD45RA^{high} T cells by ABO21009, in particular, the naive cell clusters (Figure 7E). In contrast, B cell subsets remained largely unaffected (Figure 7C). We observed the upregulation of 388 genes in T cells and only 28 in B cells following ABO21009 treatment. Importantly, no transcriptomic changes indicative of T or B cell activation were observed, aligning with results showing no cytokine release upon ABO21009 treatment (Figure 7G). Indeed, cytokine release assays performed in whole blood and PBMCs from seven healthy donors, showed no significant increase in pro-inflammatory cytokines (TNF-α, IFN-γ, IL-6, and IL-8 in whole blood or IL-2 and IL-13 in PBMC), and levels comparable to those of Erbitux, a clinically approved antibody with a low risk of cytokine release syndrome. IL-10 levels also remained unchanged (Figures 7G and S9). In addition, *ex vivo* recall assays using CEFT peptide stimulation of PBMCs from cytomegalovirus-seropositive donors revealed preserved antigen-specific CD4$^+$ and CD8$^+$ memory T cell responses in the presence of ABO21009, contrasting with the inhibition observed with tacrolimus (Figure S10). These results support a mechanism of selective depletion restricted to CD45RC^{high} cells, sparing memory and regulatory populations, and confirm the minimal off-target immunomodulatory impact of ABO21009. These findings also highlight distinct transcriptional programs triggered in T and B cells by ABO21009, warranting further investigation into their functional implications.

Although monocytes predominantly expressed low or undetectable levels of CD45RC (Figure S8C) and showed no depletion following ABO21009 treatment, we observed subtle transcriptomic changes in monocyte populations. These changes could be attributable to Fc binding of ABO21009, as previously demonstrated in ADCP assays, or activation by apoptotic cells or immune complexes. However, these alterations were not associated with significant monocyte activation or inflammatory gene signatures but rather with differentiation pathways (data not shown), shown also in the absence of cytokine release (Figure S8C), further confirming the absence of broad off-target effects. NK cells, which also express high levels of CD45RC, showed reduced CD45RC expression following treatment (Figure S8D). Although their total abundance was not decreased, these findings suggest a partial impact on NK cells, yet without major transcriptional activation under the tested conditions.

These results demonstrate the specificity of ABO21009 in depleting CD45RA^{high} T cells without inducing activation in broader T or B cell populations. This broad single-cell analysis reinforces its safety and efficacy as a targeted therapeutic drug candidate.

DISCUSSION

T and B cells play pivotal roles in the adaptive immune response, and their aberrant activation and dysregulation in autoimmune diseases lead to a loss of self-tolerance, driving the production of autoantibodies and autoreactive T cells. Thus, increasing evidence supports targeting T and B cells as a promising approach for autoimmune diseases management, offering the potential for long-term efficacy and disease remission.[24] However, no current therapeutic strategy simultaneously targets both T and B cells, while preserving Tregs, which are indispensable players in the long-term management of autoimmune diseases for maintaining immune tolerance.[25] An integrating approach combining the depletion of pathogenic T and B cells with the preservation or enhancement of Treg function represents an ideal strategy to dampen autoimmune responses while promoting immune balance and tolerance restoration, crucial for sustained disease remission and minimizing relapses and off-target effects of traditional immunosuppressors.

CD45RC, an isoform of CD45, is a promising therapeutic target due to its specific expression pattern. It is highly expressed on Th1 precursors, Th1 and TEMRA T cells, and most B cells while being absent on Treg cells.[8–10,12,16,17] This differential expression underpins its utility in selectively targeting pathogenic immune cells without impairing Treg populations. Preclinical studies using an anti-CD45RC mAb (clone OX22) with a mouse IgG1 backbone and thus with low Fc-mediated effector functions[26] demonstrated efficacy *in vivo* in preventing or treating animal models of autoimmune or inflammatory diseases such as APECED,[17] Duchenne muscular dystrophy,[16] transplant rejection,[8] and aGvHD.[10] These studies highlighted that transient depletion of CD45RC^{high} T cells,

(E) Schematic of the protocol for CD34$^+$ humanized NSG mice: 5-week-old NSG mice were irradiated with 1.5 Gy 4–6 h prior to IV injection of 50,000–120,000 CD34$^+$ human cells. After 100–150 days, when engraftment was confirmed, mice were treated IV with 1 (n = 12) or 0.05 (n = 7) mg/kg ABO21009 or PBS (n = 11) via IV injection. (F) Blood samples were analyzed by flow cytometry to quantify CD45RC^{high} T and B cell levels (data presented as absolute count of cells per μL blood). Data are provided as mean (SD) and were assessed with a two-way ANOVA with Sidak's multiple comparison test (*$p < 0.05$; **$p < 0.01$; ***$p < 0.001$; ****$p < 0.0001$).

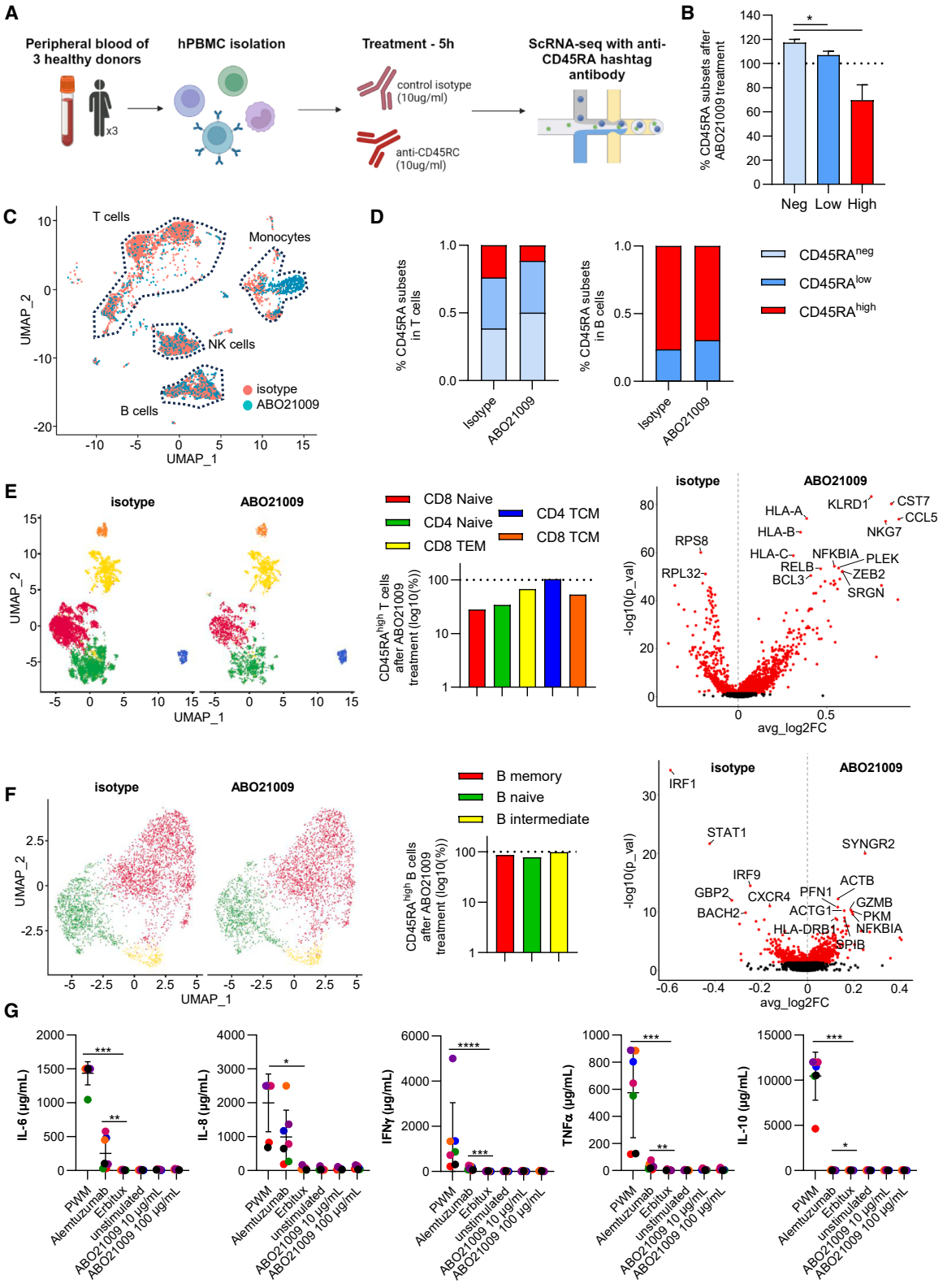

(legend on next page)

functional inhibition of B cells, and a transient increase in Treg cell numbers and antigen-specific function contributed to long-term immune tolerance.

In regard to the clinical translation, the choice of mAb backbone is critical to ensure optimal binding affinity, specificity, and activity, as these factors directly influence therapeutic efficacy, half-life, stability, and dosing frequency.[27] In this study, we investigated the MoA of chimeric and humanized anti-human CD45RC mAb with a fully functional IgG1 Fc part. Indeed, many US Food and Drug Administration/European Medicines Agency-approved therapeutic antibodies are based on a human IgG1 backbone that demonstrates efficacy as well as half-life and Fc receptor binding and are well validated in humans for safety and efficacy in various clinical indications, including autoimmune diseases.[28]

After administering a humanized version of this mAb, we demonstrated a dose-dependent depletion of both CD45RA^{high} T and B cells *in vitro* and *in vivo,* with prolonged depletion in a xenogeneic aGvHD model and CD34^{+}-reconstituted humanized mice. The recovery kinetics of CD45RA^{high} T and B cells in CD34^{+}-reconstituted humanized mice revealed a faster repopulation of B cells compared to T cells, potentially linked to the absence of thymus in these mice or to inherent differences in T versus B cell properties.[29] A similar delayed recovery of T cells relative to B cells has been observed with other depleting antibodies, such as alemtuzumab, in multiple sclerosis patients, where B cells typically recover within 3–6 months, while CD8^{+} and CD4^{+} T cell recovery can take over 2 and 5 years, respectively, likely due to increased susceptibility to apoptosis.[30–32] In contrast, ATG leads to sustained T cell depletion, particularly naive subsets, with more limited or variable effects on B cells, NK cells, and monocytes, which often remain relatively stable after administration.[33–35]

Our findings support direct apoptosis-induced cytotoxicity by binding to CD45RC as a key mechanism in CD45RA^{high} T and B cell depletion, supporting previous results obtained with the anti-CD45RC Fc-inactive mAb backbone. However, the action on B cells was only of transient blockade of activation with the Fc-inactive mAb, whereas transient depletion of B cells by the human IgG1 backbone ensures robust removal of autoreactive cells contributing to autoimmune disease pathogenesis.[6] Inactivation might allow some pathogenic cells to persist and potentially reactivate, ensuring a more robust and lasting effect in B cell-mediated autoimmune diseases.

Further mechanistic analysis revealed a predominant role for ADCP. The lack of evidence for *in vitro* ADCC and CDC activity may be explained by the elongated form and length of the CD45RABC/CD45RBC molecules,[36] in addition to the position of the epitope of the anti-hCD45RC mAb situated in the most distant extreme of these molecules, which may limit Fc-mediated activity of NK cells and complement. These findings align with evidence from RTX, where epitope proximity to the target cell membrane influences effector mechanism engagement with ADCC and CDC, favoring a membrane proximal epitope, while ADCP favors an epitope positioned further away from the membrane.[21] Preliminary experiments using a Fc-silent format confirmed that CD45RC binding alone can trigger direct apoptosis, but that Fc-FcγR interactions are essential for efficient ADCP. Notably, no ADCC or CDC activity was observed, even in the presence of autologous NK cells or human complement. These results support a mechanism dominated by direct apoptosis and ADCP. Sugar residues can also affect effector functions such as ADCC and CDC.[37,38] It is thus possible that glycosylation moieties attached to the Fc part of the mAb contribute to this effect. It would be interesting to explore the impact of chimeras and of different sugars in the activity of the mAb. In contrast to ADCC and CDC, ADCP relies on natural phagocytic process and has been associated with fewer safety issues such as cytokine release syndrome, which has been often associated with ADCC.[39–42] Our data also confirmed that ABO21009 does not induce cytokine release either *in vivo* in the tested animal models or *in vitro*, reinforcing its safety profile.

These results are consistent with previous studies highlighting the extensive glycosylation of CD45 and its influence on isoform-specific recognition. CD45 is known to carry multiple N- and O-linked glycosylation sites, with complex-type N-glycans and

Figure 7. Single-cell RNA transcriptomic analysis reveals selective depletion and transcriptional changes in CD45RA^{high} T and B cells following ABO21009 treatment, with minimal cytokine release

(A) Workflow schematic for scRNA-seq of hPBMCs treated with ABO21009 or isotype control mAbs. (B) Variation of CD45RA expression subsets (neg, low, and high) after ABO21009 mAb treatment compared to isotype control on total cells (*$p < 0.05$). (C) UMAP plot of single-cell gene expression profiles from PBMCs under isotype and ABO21009 mAb treatment conditions, colored by Azimuth clustering annotations (treatment condition). Each dot represents a single cell. (D) Distribution of CD45RA subsets within T and B cell populations under isotype and ABO21009 treatment conditions. (E and F) Top, UMAP plots of CD45RA^{high} T (E) and B (F) cells under isotype control (left) and ABO21009 treatment (right) conditions. Each dot represents a single cell. Center, bar plot showing the variation in CD45RA^{high} T subsets following ABO21009 treatment. Bottom, volcano plot showing differentially expressed genes in PBMCs treated with ABO21009 compared to isotype control. Each dot represents a gene, with the *x* axis displaying the log2 fold change (FC) and the *y* axis representing the −log10 adjusted *p* value. Genes with significant upregulation (adjusted $p < 0.05$ and $\log_2 FC > 1$) are highlighted in red. Non-significant genes are shown in black. Selected upregulated genes are labeled. Statistical analysis was performed using DESeq2. (G) Cytokine release study on whole blood from healthy donors ($n = 7$) was incubated for 24 h with ABO21009 (100 and 10 μg/mL), pokeweed mitogen (PWM, 100 μg/mL), and alemtuzumab (10 μg/mL) as positive controls and PBS and Erbitux (100 μg/mL) as negative controls. Plasma samples were analyzed for cytokine levels (IL-6, IL-8, IFN-γ, TNF-α, and IL-10) using high-sensitivity magnetic beads. Data are provided as mean (SD) and were assessed with a paired ratio *t* test in comparison to the Erbitux condition (*$p < 0.05$; **$p < 0.01$; ***$p < 0.001$; ****$p < 0.0001$). scRNA-seq, single-cell RNA sequencing; TCM, central memory T cell; TEM, effector memory T cell; UMAP, uniform manifold approximation and projection.

terminal sialic acids contributing to structural diversity and isoform-specific antibody binding.[43,44] Glycosylation has been shown to impact CD45 function and antibody recognition, particularly in the context of splicing isoforms and cellular activation states.[45] Our observation that anti-CD45RC mAb recognition is abolished by the removal of complex N-glycans and sialic acids but is unaffected by Endo F1 or O-glycan removal aligns with these studies and suggests that ABO21009 targets a glycoform-dependent epitope preferentially displayed on CD45RC^{high} subsets. Similar glycan-dependent epitopes have been described for other immunologically relevant targets, where both glycan composition and spatial presentation modulate antibody specificity and binding affinity.[46] These findings reinforce the importance of glycan context in epitope formation and have implications for antibody-based therapies targeting glycosylated surface molecules. Importantly, while some inter-individual variability in ABO21009 binding was observed among T cells from healthy donors, B cells showed consistent reactivity. Moreover, previously published studies in autoimmune patients confirmed stable CD45RC expression and mAb binding across individuals,[17] supporting the clinical relevance and robustness of the targeted glyco-epitope.

Unlike other existing therapeutic mAbs targeting specific populations such as CD20 (B cell marker), CD52 (pan-leukocyte antigen), CD3 (T cell marker) or specific cytokines (i.e., TNF-α), ABO21009 offers a novel dual-targeting approach. By selectively depleting pathogenic T and B cells while preserving Treg cells, this strategy addresses key limitations of traditional immunosuppressants, such as systemic side effects and nonspecific immunosuppression. Although not directly compared here, antibodies targeting other CD45 isoforms such as CD45RA may lack the selectivity of CD45RC, especially for sparing Tregs. The broader expression of isoforms such as CD45RB also limits their therapeutic specificity.

The *in vivo* efficacy of ABO21009 in both xenogeneic aGvHD and humanized immune system models supports its potential as a targeted immunomodulatory therapy. The dose-dependent protection observed in the aGvHD model, along with the corresponding depletion of CD45RA^{high} T and B cells, underscores the functional relevance of targeting these subsets in controlling pathogenic immune responses. While survival differences between dose groups were not strictly proportional, this may reflect the rapid and aggressive kinetics of the xenogeneic aGvHD model, which can obscure finer resolution of dose-response relationships. Nonetheless, a minimal effective dose (0.05 mg/kg) was identified that consistently delayed disease onset and improved survival. Additionally, this xenogeneic aGvHD model is heavily T cell-driven due to the lack of functional B, NK, and myeloid compartments in the host, which may overestimate the contribution of T cell depletion to therapeutic efficacy compared with the complexity of human disease, where these immune populations also play important roles.[47] Importantly, PD studies in CD34^{+}-reconstituted humanized NSG mice demonstrated rapid and selective depletion of CD45RA^{high} T cells at therapeutically effective doses in the aGvHD model, highlighting a correlation between depletion kinetics and protection. The more prolonged depletion of T cells relative to B cells and the sparing of CD45RA$^{low/neg}$ populations highlight the precision of ABO21009 in modulating specific immune compartments without inducing broad lymphopenia. These findings suggest that ABO21009 may offer a favorable balance between efficacy and immune preservation, with a recovery profile that may reduce the risk of long-term immunosuppression. In line with previous reports,[8–10,17] our data indicate that regulatory T cells, which typically express low/neg levels of CD45RC, are relatively preserved following treatment, supporting the selective action of the antibody and its potential for maintaining immune tolerance. Supporting this, functional recall responses to viral and bacterial antigens were preserved *ex vivo* in ABO21009-treated PBMCs, confirming the integrity of memory T cell function. Combined with the absence of cytokine release and pro-inflammatory transcriptional changes, these results indicate a mechanism that selectively eliminates pathogenic effectors while maintaining protective immunity, supporting the potential of ABO21009 not only to avoid immunodeficiency but also to promote durable immunomodulation and tolerance induction.

While the xenogeneic aGvHD and CD34^{+} humanized mouse models provide valuable insights into the PD and immune-depleting properties of the anti-CD45RC mAb, they present inherent limitations in fully recapitulating the complexity of human immune responses. These models lack key components such as fully functional secondary lymphoid structures, human cytokine networks, and a complete myeloid compartment, which may influence immune cell interactions and therapeutic outcomes. Consequently, although our findings demonstrate robust T and B cell depletion and prevention of aGvHD *in vivo*, the translational implications should be interpreted cautiously. Further validation in early-phase clinical trials will be essential to fully assess the efficacy, selectivity, and safety of this therapeutic approach in humans.

While this study primarily focused on the depletion of pathogenic T and B cells, it is important to note that CD45RC^{high} expression is also found on other subsets of cells such as NK cells[10] and that their respective contribution to the proposed mechanism of action of anti-CD45RC mAb is unknown. Maintaining NK cell function is crucial, as these cells contribute to antiviral defense and tumor surveillance; however, even in clinical contexts where NK cell function is absent, such as in patients with deficiencies, individuals were not susceptible to infections and can maintain overall health with appropriate medical management, suggesting that transient or partial modulation of NK cell activity is unlikely to pose significant risks.[48,49] In addition, several studies described the absence of expression of CD45RA by immature and activated NK cells, and although CD45RC was not analyzed, this suggests that some NK cell subsets such as the activated or cytotoxic subsets could be CD45RC$^{low/neg}$.[50–54] The potential depletion of alternative pathogenic cell subsets by anti-CD45RC mAb could provide a broader immunomodulatory effect, extending the therapeutic benefits of this approach beyond T and B cell targeting.

In conclusion, this work has important implications beyond proof of concept, highlighting the potential of this new class of targeted immunotherapies to harness the regulatory ability of Treg cells in the clinic with the possibility of achieving sustained disease remission. The recent successes of CD19-targeting chimeric antigen receptor-T cells in autoimmune diseases such as lupus highlight the therapeutic potential of B cell depletion, although their complexity and long-term immunosuppressive effects may limit broad applicability. The anti-CD45RC mAb offers a complementary, off-the-shelf approach that selectively targets pathogenic T and B cells while sparing Tregs, with a more favorable safety and accessibility profile. However, challenges remain, including ensuring long-term safety, managing inter-patient variability in responses, and addressing the complexity of immune regulation in diverse autoimmune conditions and the requirement for rigorous clinical studies to confirm efficacy and safety in humans.

MATERIALS AND METHODS

Antibodies

The chimeric anti-CD45RC, ABIS-45RC, possesses murine variable regions and human constant regions. It was derived from a murine antibody (IgG1/k) against CD45RC and is produced in Chinese hamster ovary (CHO) DG44 cells. An afucosylated variant, referred to as ABIS-45RC^{aF}, was generated using fucose-deficient CHO cells to enhance FcγR binding. Humanization of this anti-CD45RC mAb was achieved through grafting complementarity determining regions (CDRs, defined by the Kabat nomenclature) into human germline antibody sequences to produce the ABO21009 mAb.

Antibodies used for treatments *in vitro* and *in vivo* are described in Table S5. Antibodies used for flow cytometry experiments are described in Table S6.

N-glycan profiling

Glycosylation analysis was performed by Abzena using hydrophilic interaction liquid chromatography with fluorescence detection and mass spectrometry (HILIC-FLD-MS) using the Waters GlycoWorks RapiFluor-MS (RFMS) N-Glycan kit. The workflow included deglycosylation, labeling, purification, and chromatographic analysis.

For each analysis, 15 μg of a 1-mg/mL sample was heated with RapiGest, digested with PNGase F, labeled with RFMS, and purified via HILIC solid-phase extraction. The dried sample was reconstituted and analyzed with a Waters BioAccord system using an ultra-performance liquid chromatography glycan bridge ethane hybrid amide column (1.7 μm, 2.1 × 150 mm). Separation was performed using a 20%–80% acetonitrile gradient in 50 mM ammonium formate (pH 4.4) at 60°C, with FLD (265/425 nm) and MS (50–2,000 Da, positive ion mode) detection. Data acquisition was performed by referencing the RapiFluor-MS-Labeled Dextran Calibration Ladder and matching glucose unit values and masses to the RFMS glycan MS library. Relative glycan quantification was based on area under the curve in HILIC-FLD, with manual MS-based verification when needed.

Cell isolation and culture

Blood was collected at the Etablissement Français du Sang (Nantes, France) from healthy donors. Written informed consent was provided according to institutional guidelines. PBMCs were purified from blood by Ficoll-Paque density-gradient centrifugation (Eurobio). An AutoMACS Pro was used to magnetically sort T cells (pan T cell isolation kit, Miltenyi Biotec), B cells (B cell isolation kit, Miltenyi Biotec), NK cells (NK cell isolation kit, Miltenyi Biotec), and monocytes (classical monocyte isolation kit, Miltenyi Biotec) as stated by the kit supplier.

Daudi, THP-1, and MOLT-4 cell lines were purchased from American Type Culture Collection (ATCC) and cultured in complete RPMI (Gibco, Thermo Fisher Scientific): RPMI plus 10% fetal bovine serum (Gibco, Thermo Fisher Scientific), 100 U/mL penicillin-streptomycin (Gibco, Thermo Fisher Scientific), and 2 mM glutamine (Sigma-Aldrich), in a 37°C 5% CO_2 incubator.

Monocyte-derived macrophages were obtained after isolated CD14$^+$ monocytes were cultured in 50 ng/mL M-CSF (Miltenyi Biotec) complete RPMI for 5 days in a 37°C CO_2 incubator. For cytometry experiments, macrophages were harvested after PBS wash and 5-min incubation in TripleX (Gibco, Thermo Fisher Scientific).

CD45RC cell membrane density quantification

Fresh PBMCs were isolated from whole blood by Ficoll-Paque density-gradient centrifugation (Eurobio). The remaining red blood cells and platelets were eliminated with a hypotonic solution. The cells were then washed, re-suspended in PBS-fetal calf serum (FCS)-2%-1 mM EDTA, and counted. To identify sub cells, single-cell suspensions were stained with cell-specific markers, including anti-CD3 PE- cyanine 7 (Cy7), anti-CD19 PerCp-Cy5.5, anti-CD56 allophycocyanin (APC)-Cy7, anti-CD45RC PE (ABO21009), anti-CD4 fluorescein isothiocyanate (FITC) antibodies, and 4′,6-diamidino-2-phenylindole (DAPI, Sigma-Aldrich). The number of CD45RC molecules per cell were determined using the Quantibrite-bead reference standard approach after coupling of the CD45RC mAb with PE. Via a linear standard curve obtained with BD Biosciences PE Beads, the geometric mean could be obtained. The sizes of the cells were assessed using the Flow Cytometry Size Calibration Kit (Thermo Fisher Scientific), which allowed the calculation of CD45RC molecules per μm^2 of membrane. In addition to fresh PBMCs, cells from different cell lines (Daudi and MOLT-4) were stained with anti-CD45RC PE (ABO21009) and DAPI. Analysis was performed on a BD FACS Verse with FACSuite Software version 1.0.6. Post-acquisition analysis was performed using FlowJo software.

Western blot

The human CD45RABC recombinant protein is produced in CHO cells and glycosylated (hrCD45RABC, catalog no. 1430-CD-050, R&D Systems). When necessary, it was deglycosylated under denaturing or native conditions with enzymes (endoglycosidase F1, PNGase F, O-glycosidase, α-2(3,6,8,9)-neuraminidase) from the

EDEGLY kit (catalog no. EDEGLY-1KT, Sigma-Aldrich) according to the manufacturer's method description.

After denaturing and separation on Mini-PROTEAN TGX Precast Protein Gels (Bio-Rad), the samples were transferred to nitrocellulose membranes, which were blocked with Tris-buffered saline with 0.1% Tween 20 detergent 5% BSA (w/v) at room temperature (RT) for 2 h, followed by anti-CD45RC mAb incubation at 4°C overnight on a shaking platform. After three washes, the membranes were incubated with horseradish peroxidase (HRP)-conjugated secondary antibodies for 2 h at RT. Then, the enhanced chemiluminescence substrate kit (catalog no. 32106, Thermo Fisher Scientific) was used for the detection of HRP, and images were acquired using ChemiDoc MP Imaging System (Bio-Rad).

ELISA binding assay

The binding activities of anti-CD45RC mAb variants (IgG1 ABIS-45RC and ABIS-45RC^{aF}) were tested against hrCD45RABC protein in an ELISA assay. Briefly, CD45RABC (R&D Systems, 1.5 μg/mL) was coated on to a Maxisorp plate and incubated overnight at 4°C. Unbound protein was washed away with PBS-T (0.05% Tween 20 in PBS) and blocked with PBS 5% BSA for 2 h at RT. Plates were washed with PBS-T, and a dose range of anti-CD45RC or ABIS-45RC^{aF} mAbs was added to the wells and incubated at RT for 2 h. Plates were washed with PBS-T and incubated with a secondary donkey anti-IgG H + L peroxidase-labeled antibody (Jackson Immunoresearch), which was then incubated at RT for 1 h. Plates were washed with PBS-T and incubated with 3,3′,5,5′-tetramethylbenzidine (BD OptEIA) substrate solution for 5 min. The reaction was stopped with H_2SO_4 (Merck) solution and absorbance was then measured at optical density 450 using a TECAN Spark 10M reader.

FACS binding assay

The binding activities of anti-CD45RC mAb variants (IgG1 ABIS-45RC and afucosylated ABIS-45RC^{aF}) were tested against cell membrane bound CD45RC protein in a fluorescence-activated cell sorting (FACS) assay. After an Fc blocking incubation, frozen PBMCs were incubated for 1 h on ice with a dose range of ABIS-45RC or ABIS-45RC^{aF} Abs. Cells were washed and stained with anti-CD3 PE-Cy7 anti-CD56 APC-Cy7, anti-CD19 PercPCy5.5, anti-CD14 V500 anti-human IgG FITC antibodies for 30 min on ice. Cells were then washed, resuspended in a DAPI solution, and acquired on an Aurora flow cytometer (Cytek).

Antibody interaction analysis by surface plasmon resonance

Surface plasmon resonance (SPR) interaction analyses were carried out on a Biacore T200 instrument (Cytiva) at 25°C using sensor chips CM3 (Cytiva) and running buffer HBS-EP+ (10 mM HEPES pH 7.4, 150 mM NaCl, 3 mM EDTA, 0.05% Tween 20) (Biaffin). An anti-His-tag capture approach via covalently immobilized anti-His antibody was applied to reversibly immobilize the His-tagged antigen rhCD45ABC in low surface density. The anti-CD45RC antibodies were injected as analytes in the single-cycle kinetic (SCK) mode to quantitatively characterize the interaction with rhCD45RABC. Five serial 3-fold dilutions of anti-CD45RC antibodies (3.7, 11.1, 33.3, 100, and 300 nM) were injected (50 μL/min) consecutively for 180 s each, and the dissociation was recorded for 600 s. Complete regeneration of the anti-His capture surfaces was accomplished by injecting 10 mM glycine (pH 1.5) following 3 M guanidine hydrochloride (30 s at 20 μL/min, respectively). Upon double referencing (control surface without rhCD45RABC and buffer blank subtraction), the recorded binding data, displaying two distinguishable binding events, were fitted to the heterogeneous ligand binding model provided in the Biacore T200 evaluation software (Cytiva).

Cytotoxicity assays (direct apoptosis-induced cytotoxicity, crosslinking, and CDC)

Fresh PBMCs were stored overnight in complete RPMI at 4°C, then incubated with a dose range of anti-CD45RC antibodies or a single dose of ATG (Sanofi), RTX (Roche), or IgG1 isotype as controls, diluted in complete RPMI for 2.5 h in a 37°C CO_2 incubator. After a washing step, cells were stained with anti-CD3 PE-Cy7, anti-CD56 APC-Cy7, anti-CD19 PercPCy5.5, and anti-CD45RA PE antibodies for 30 min on ice. After a PBS washing step, cells were stained with annexin V APC for 20 min at RT. DAPI was added to the wells, and the cells were acquired on an Aurora flow cytometer (Cytek).

For CDC experiments with rabbit serum, 10% rabbit serum containing active complement (Sigma) was added with the anti-CD45RC antibodies' dose range, ATG, or isotype control wells. For CDC experiments with human complement, 5% human plasma (pooled from several donors, Eurobio) containing active complement or 5% decomplemented human plasma was used.

For crosslinking experiments, an anti-IgG/IgM secondary antibody (Thermo Fisher Scientific) at a constant 250-fold dilution was added with the anti-CD45RC mAbs dose range, ATG, or isotype control wells.

Data are expressed as the percentage of specific killing, which takes into account cell death as well as apoptosis normalized on the isotype condition.

ADCC

Isolated T or B cells from fresh PBMCs were co-incubated with isolated autologous NK cells for 4 h in a 37°C CO_2 incubator, in the presence or absence of a dose range of anti-CD45RC antibodies or a single dose of ATG, RTX, or IgG1 isotype as controls, diluted in complete RPMI. After a washing step, cells were stained with anti-CD3 PE-Cy7/PE-CF594 or anti-CD19 PercPCy5.5, and anti-CD56 APC-Cy7 plus anti-CD45RA PE/FITC antibodies for 30 min on ice. In related experiments, anti-CD107a PE was added to the mix for NK degranulation quantification. For apoptosis detection, after a PBS washing step, cells were stained with annexin V APC for 20 min at RT. DAPI was added to the wells, and the cells were acquired on an Aurora flow cytometer (Cytek). Data are expressed as the percentage of specific killing, which takes into account cell death as well as apoptosis normalized on the isotype condition.

Lentivirus production

Plasmids recombinant for CD45RA, -RB, -RC, and -RO were produced internally and verified by enzymatic digestion. The plasmid recombinant for CD45RABC was purchased from Vectorbuilder. Packaging plasmids pMDLg/pRRE and pRSV-Rev and envelope plasmid pMD2-G were purchased from Addgene. Briefly, HEK293T (ATCC) were seeded in Dulbecco's modified Eagle's medium (DMEM, Thermo Fisher Scientific) and 10% FCS and transfected with plasmids, using $CaCl_2$. The day after, cells were washed and then cultured in advanced DMEM (Thermo Fisher Scientific) free of FCS. At days 2 and 3 after transfection, the supernatant was harvested, 0.45 μm filtered, concentrated by a 90-min 25,000 rpm spin, and stored at −80°C. Lentivirus titration was performed on HEK cells. Briefly, 25,000 HEK cells were seeded in flat-bottom 24-well plates with a range of lentivirus volumes. Transduction efficiency was assessed by anti-CD45RC staining with a fluorescent antibody after 3 days of culture by flow cytometry, and the concentration of infectious particles was calculated.

MOLT-4 and HEK transduction

In regard to MOLT-4, 10^6 cells were distributed at 10^5 cells per well in flat-bottom p96 plates in complete RPMI. After centrifugation for 1 min at 2,500 rpm, the supernatant was removed, and lentivirus CD45RABC (Vectorbuilder) was added at MOI 20 and incubated for 4 h at 37°C. Then, cells were kept in culture for 1 week at a maximum of 2×10^6 cells/mL. After 2 weeks, cells were sorted on an ARIA cell sorter (BD Biosciences) gating on $CD45RC^{high}$. This procedure was repeated 8 times to obtain an acceptable CD45RC expression at the surface of the cells.

In regard to HEK, cells were plated in a P12 well flat bottom at 0.1×10^6 cells per well in 1000 μL of DMEM 10% FCS 1% penicillin-streptomycin 1% L-glutamine. The desired lentivirus (CD45RA, CD45RB, CD45RC, CD45RO, and CD45RABC) was added at an MOI of 10, expect for CD45RC for which MOI was at 0.6, and cells were incubated overnight at 37°C 5% CO_2. After 1 day, the medium was changed, and cells were kept in culture at a maximum concentration of 0.5×10^6 cells/mL.

ADCP

ADCP was measured as described before.[55] Briefly, target cells (isolated T, B, and NK cells, total PBMC, Daudi, or CD45RC-transduced MOLT-4 cells) were stained with 0.05 μM CFSE (Thermo Fisher Scientific). Effector cells (monocyte-derived macrophages or THP-1 cells) were stained with 5 μM CPD-eFluor670 (Thermo Fisher Scientific). Target and effector cells were then co-incubated in the presence or absence of a dose range of ABIS-45RC or $ABIS\text{-}45RC^{aF}$ mAbs or IgG1 isotype as a negative control for 1 h in a 37°C CO_2 incubator. Cells were then acquired on a Canto flow cytometer (BD Biosciences).

Microscopy

Monocytes-derived macrophages were cultured in IBIDI plates. On the fifth day, CFSE-labeled Daudi cells were opsonized with 10 μg/mL anti-CD45RC humanized antibody and put in contact with the macrophages for 2 h Non-phagocytosed Daudi cells were flushed out with complete RPMI, and IBIDI plates were imaged with a confocal microscope (Nikon). Macrophages and remaining phagocytosed Daudi cells were numbered using Fiji software.

Mice

The NSG mice were bought from Charles River and housed in our animal facilities in specific pathogen-free conditions (UTE IRS-UN), and this study was carried out according to permit numbers APAFIS 22702 and APAFIS 30067 from the Ministry of Research.

Xenogeneic aGvHD

Eight-week-old NSG female mice were 1.5 Gy irradiated. Six h later, they were IV injected with 1.5×10^7 fresh PBMCs from healthy volunteers and concomitantly IP injected with 4 different doses (0.2, 0.8, 3.2, and 12.8 mg/kg 3 times per week for 3 weeks) of anti-CD45RC mAb or PBS vehicle as a negative control. GvHD development was evaluated every other day at least by body weight loss and clinical scoring (Table S7) and every 14 days by hPBMC engraftment monitoring in blood by flow cytometry (viability V500, anti-CD3 PE-CF594, anti-CD19 V450, anti-CD56 BV605, anti-hCD45 BUV395, anti-CD45RA FITC, anti-CD4 SparkNIR685, anti-murine CD45 APC-Cy7, anti-CD127 PE, and anti-CD25 APC; see Table S6 for details). hPBMC engraftment was also assessed in blood and spleen at sacrifice.

$CD34^+$ humanized model

Five-week-old NSG female mice were 1.5 Gy X-ray irradiated, and 6 h later, they were IV injected with 50–150,000 thawed $CD34^+$ cells (Lonza) from cord blood. After 100–250 days, differentiation of different human mononuclear cell subsets was assessed by flow cytometry. When $hCD45^+$ cells were superior to 60% of all PBMCs (mouse $CD45^+$ + human $CD45^+$), mice were IP injected with 0.8 mg/kg ABIS-45RC mAb, anti-CD3 OKT3, anti-CD20 RTX, or PBS as a negative control or IV injected with 0.05 or 1 mg/kg ABO21009 or PBS as a negative control. hPBMC depletion was then measured by flow cytometry in the blood, bone marrow (from both femurs), and spleen at sacrifice (viability eF506, anti-CD3 PE-CF594, anti-CD19 V450, anti-CD14 BUV737, anti-CD56 BV605, anti-CD45 BUV395, anti-CD45RA APC, anti-CD4 SparkNIR685, anti-FoxP3 PE, and anti-murine CD45 APC-Cy7; see Table S6 for details).

$CD34^+$ cells were tested for CD45RC expression: after labeling with a viability dye VD450, we added the staining antibodies cocktail (anti-hCD45 APC-Cy7, anti-hCD34 PECy7, anti-hCD38 Percp-Cy5.5, and anti-hCD45RC FITC). Cells were mixed and incubated on ice for 30 min. Fluorescence was measured with a Canto II (BD Biosciences) and analyzed with FlowJo software (Tree Star).

Human cytokines in mice plasma

To determine the human cytokine concentrations in plasma of immune-humanized NSG mice, analysis was carried out using the

Ella Simple Plex system (Protein Simple Kit, Biotechne SAS) for IFN-γ, TNF-α, IL-6, IL-10, IL-2, IL-13, and granzyme B (Simple Plex cartridges, reference no. SPCKE-PS-006151). Mice plasma were diluted 2-, 3-, or 4-fold depending on available volume. The assay was run per the manufacturer's instructions.

scRNA-seq

Freshly isolated PBMCs of three healthy donors were labeled with anti-human Hashtag antibodies TotalSeq-C (BioLegend) and were pooled together. Cell viability was >90%. Then, cells were labeled with anti-CD45RA CITE-seq mAbs (HI100 clone). Single-cell libraries were performed according to Chromium Next GEM Single Cell 5′ Reagent Kits v2 protocol (10x Genomics). Cell suspensions were loaded onto chromium single-cell chip K in 4 different wells (20,000 cells per well) and run immediately on the Chromium controller (10x Genomics). Two libraries were prepared for mRNA (RNA) and for barcoded antibodies (hashtag oligos [HTO] and CITE-seq). They were sequenced with NovaSeq 6000 (Illumina) according to 10x Genomics' recommendations. In parallel, the PBMCs were tested in an apoptosis assay as described above.

scRNA-seq data analysis

For primary analysis, FASTQ files generated from BaseCalling (BCL) files with CellRanger package (version 6.1.2) were demultiplexed and aligned to a human reference genome (hg38). The CITE-seq-Count function (version 1.3.4) was used to count antibody hashtag sequences.

For the secondary analysis, count matrixes were analyzed with the Seurat R package (version 4.1.1). Cells with more than 10% of mitochondrial genes were excluded. Gene expression was log normalized and scaled. HTO expression was normalized and demultiplexed. Doublet cells and negative cells for HTO were removed. Downstream analysis was performed on 67806 single cells. On average, 1577 genes were expressed per cell in fresh PBMCs. A nonlinear dimensionality reduction UMAP and a clustering were performed to visualize distinct cell clusters with a resolution of 0.005. Differentially expressed genes were calculated using the "wilcox" method to characterize marker genes of each cell cluster implemented in the Seurat package's "FindAllMarkers" or "FindMarkers" functions. CITE-seq antibodies gates were set up according to expression profiles detected by flow cytometry with negative and positive fractions and for some CITE-seq antibodies including anti-CD45RA mAb with neg, low, and high fractions.

Biacore SPR analysis of binding to human Fcγ receptors (FcγR and FcRn)

The ability of ABO21009 and a control mAb (trastuzumab) to bind to different FcγRs was determined by Abzena using Biacore SCK analysis using a Biacore T200 instrument running Biacore T200 evaluation software (Cytiva) running at a flow rate of 30 μL/min. FcγRs were captured on a CM5 sensor chip pre-coupled with a His capture kit (Cytiva) using standard amine chemistry. The human (h) Fc receptors, hFcγRI, hFcγRIIA (both 167Arg and 167His polymorphisms), hFcγRIIB, hFcγRIIIA (both 176Phe and 176Val polymorphisms), and hFcγRIIIB were obtained from Sino Biological.

The ability of the test samples to bind to FcRn was determined using Biacore multi-cycle kinetic (MCK) analysis using a Biacore T200 instrument running Biacore T200 evaluation software (Cytiva) running at a flow rate of 30 μL/min. Human FcRn was captured on a CM5 sensor chip pre-coupled using a His capture kit (Cytiva) using standard amine chemistry. The human FcRn was obtained from Sino Biological.

Cytokine release study

The cytokine release study was done by Abzena. Whole blood from seven healthy donors was used immediately upon receipt. ABO21009 was tested in the assay at 100 and 10 μg/mL. Pokeweed mitogen (PWM) (Sigma-Aldrich) was used as a positive control at 100 μg/mL. Negative control cultures were established in which whole-blood cultures were treated with PBS. Clinical antibodies alemtuzumab (Lemtrada, Evidentic) and Erbitux (Evidentic) were used at final assay concentrations of 10 and 100 μg/mL, respectively. We added 20 μL of each sample to a 96-well plate in duplicate followed by 180 μL fresh whole blood. Plates were then incubated at 37°C with 5% CO_2 for 24 h. Aliquots of plasma were taken from the cultures after 24 h of incubation. Plasma samples were analyzed for cytokine levels (IL-6, IL-8, IFN-γ, TNF-α, and IL-10) using high-sensitivity magnetic Milliplex kits (Merck Millipore), according to the manufacturer's instructions. Plasma samples and serially diluted standards were incubated with pre-mixed capture beads for 16–18 h, followed by additional incubation with detection reagents. Data were acquired using a FLEXMap 3D (Bio-Rad). Cytokine secretion levels were determined in pg/mL from a standard curve using xPONENT software (Bio-Rad).

Statistical analysis

Data were analyzed using GraphPad Prism (version 10) and represented as mean ± standard deviation (SD), with $^{*}p < 0.05$, $^{**}p < 0.01$, $^{***}p < 0.001$, and $^{****}p < 0.0001$. EC_{50} was calculated through a four-parameter sigmoid regression analysis of curves obtained from raw data. Differences between groups were assessed using one-way ANOVA for one-parameter graphs, with several conditions compared with Dunn's multiple comparison tests. Two-way ANOVA was used for two-parameter graphs (curves), with several conditions compared with Sidak's multiple comparison tests. Differences between two groups with one-parameter data were assessed using the Mann-Whitney statistical test for unpaired or below $n = 5$ data or Wilcoxon statistical tests for paired data. Survival was analyzed by the Mantel-Cox log rank test. Cytokine release study data were compared using a ratio paired t test, and significance was compared against cytokine concentration in response to Erbitux condition.

DATA AND CODE AVAILABILITY

All relevant data supporting the findings of this study are available within the article and its supplemental information files. Raw datasets are available from the corresponding

author upon reasonable request. Single-cell transcriptomic data have been deposited in a public repository ArrayExpress accession number E-MTAB-15576, in compliance with journal policies.

ACKNOWLEDGMENTS

This work was funded by AbolerIS Pharma, the Labex IGO (ANR-11-LABX-0016-01), the Agence Nationale de la Recherche PRC (18-CE18-0024-02), the I-SITE NExT (ANR-16-IDEX-0007), and the Agence de la Biomedecine. AbolerIS Pharma was further supported by the iLab program (DOS0162058) and the REACT-EU initiative (PL0032023). We thank Pascal Merchiers, Ann Meulemans and the team at AbolerIS Pharma for their constructive discussions and valuable insights. We acknowledge Steven Nedellec and Philippe Hulin from the MicroPICell core facility (SFR Bonamy, BioCore, Inserm UMS 016, CNRS UAR 3556, Nantes, France), a member of the Scientific Interest Group (GIS) Biogenouest, IBISA, and the national infrastructure France-Bioimaging supported by the French national research agency (ANR-10-INBS-04). We acknowledge Cécile Braudeau from the CIMNA platform (SFR Bonamy, Nantes, France). We acknowledge Julien Drochon and his team from the UTE IRS-UN platform.

AUTHOR CONTRIBUTIONS

C.G. and C.B. wrote the first draft of the manuscript. C.G. and I.A. designed, funded, and analyzed the data. C.B. designed and performed research and analyzed the data. G.A.-B., L.-H.O., N.V., A.S., R.H., and L.T. performed the research and analyzed the data. A.C., K.S., and R.V.B. designed and analyzed the data. All the authors reviewed and approved the manuscript.

DECLARATION OF INTERESTS

C.G. and I.A. have patents and ownership interests in the startup company AbolerIS Pharma. C.G., C.B., N.V., G.A.-B., K.S., A.C., and R.V.B. are employees or consultants of AbolerIS Pharma.

SUPPLEMENTAL INFORMATION

Supplemental information can be found online at https://doi.org/10.1016/j.ymthe.2025.10.057.

REFERENCES

1. Sakaguchi, S., Sakaguchi, N., Asano, M., Itoh, M., and Toda, M. (1995). Immunologic self-tolerance maintained by activated T cells expressing IL-2 receptor alpha-chains (CD25). Breakdown of a single mechanism of self-tolerance causes various autoimmune diseases. J. Immunol. *155*, 1151–1164.

2. Sakaguchi, S., Yamaguchi, T., Nomura, T., and Ono, M. (2008). Regulatory T cells and immune tolerance. Cell *133*, 775–787. https://doi.org/10.1016/j.cell.2008.05.009.

3. Bailey-Bucktrout, S.L., Martinez-Llordella, M., Zhou, X., Anthony, B., Rosenthal, W., Luche, H., Fehling, H.J., and Bluestone, J.A. (2013). Self-antigen-Driven Activation Induces Instability of Regulatory T Cells during an Inflammatory Autoimmune Response. Immunity *39*, 949–962. https://doi.org/10.1016/j.immuni.2013.10.016.

4. Komatsu, N., Okamoto, K., Sawa, S., Nakashima, T., Oh-hora, M., Kodama, T., Tanaka, S., Bluestone, J.A., and Takayanagi, H. (2014). Pathogenic conversion of Foxp3+ T cells into TH17 cells in autoimmune arthritis. Nat. Med. *20*, 62–68. https://doi.org/10.1038/nm.3432.

5. Moreau, A., Varey, E., Anegon, I., and Cuturi, M.-C. (2013). Effector Mechanisms of Rejection. Cold Spring Harb. Perspect. Med. *3*, a015461. https://doi.org/10.1101/cshperspect.a015461.

6. Lee, D.S.W., Rojas, O.L., and Gommerman, J.L. (2021). B cell depletion therapies in autoimmune disease: advances and mechanistic insights. Nat. Rev. Drug Discov. *20*, 179–199. https://doi.org/10.1038/s41573-020-00092-2.

7. Kuhn, C., and Weiner, H.L. (2016). Therapeutic anti-CD3 monoclonal antibodies: from bench to bedside. Immunotherapy *8*, 889–906. https://doi.org/10.2217/imt-2016-0049.

8. Picarda, E., Bézie, S., Boucault, L., Autrusseau, E., Kilens, S., Meistermann, D., Martinet, B., Daguin, V., Donnart, A., Charpentier, E., et al. (2017). Transient antibody targeting of CD45RC induces transplant tolerance and potent antigen-specific regulatory T cells. JCI Insight *2*, e90088. https://doi.org/10.1172/jci.insight.90088.

9. Ordonez, L., Bernard, I., L'Faqihi-Olive, F.-E., Tervaert, J.W.C., Damoiseaux, J., and Saoudi, A. (2009). CD45RC Isoform Expression Identifies Functionally Distinct T Cell Subsets Differentially Distributed between Healthy Individuals and AAV Patients. PLoS One *4*, e5287. https://doi.org/10.1371/journal.pone.0005287.

10. Boucault, L., Lopez Robles, M.-D., Thiolat, A., Bézie, S., Schmueck-Henneresse, M., Braudeau, C., Vimond, N., Freuchet, A., Autrusseau, E., Charlotte, F., et al. (2020). Transient antibody targeting of CD45RC inhibits the development of graft-versus-host disease. Blood Adv. *4*, 2501–2515. https://doi.org/10.1182/bloodadvances.2020001688.

11. Xystrakis, E., Cavailles, P., Dejean, A.S., Cautain, B., Colacios, C., Lagrange, D., van de Gaar, M.-J., Bernard, I., Gonzalez-Dunia, D., Damoiseaux, J., et al. (2004). Functional and genetic analysis of two CD8 T cell subsets defined by the level of CD45RC expression in the rat. J. Immunol. *173*, 3140–3147.

12. Powrie, F., and Mason, D. (1990). OX-22high CD4+ T cells induce wasting disease with multiple organ pathology: prevention by the OX-22low subset. J. Exp. Med. *172*, 1701–1708.

13. Bézie, S., Meistermann, D., Boucault, L., Kilens, S., Zoppi, J., Autrusseau, E., Donnart, A., Nerrière-Daguin, V., Bellier-Waast, F., Charpentier, E., et al. (2018). Ex Vivo Expanded Human Non-Cytotoxic CD8+CD45RClow/− Tregs Efficiently Delay Skin Graft Rejection and GVHD in Humanized Mice. Front. Immunol. *8*, 2014. https://doi.org/10.3389/fimmu.2017.02014.

14. Xystrakis, E., Dejean, A.S., Bernard, I., Druet, P., Liblau, R., Gonzalez-Dunia, D., and Saoudi, A. (2004). Identification of a novel natural regulatory CD8 T-cell subset and analysis of its mechanism of regulation. Blood *104*, 3294–3301. https://doi.org/10.1182/blood-2004-03-1214.

15. Xystrakis, E., Bernard, I., Dejean, A.S., Alsaati, T., Druet, P., and Saoudi, A. (2004). Alloreactive CD4 T lymphocytes responsible for acute and chronic graft-versus-host disease are contained within the CD45RC ^{high} but not the CD45RC ^{low} subset. Eur. J. Immunol. *34*, 408–417. https://doi.org/10.1002/eji.200324528.

16. Ouisse, L.-H., Remy, S., Lafoux, A., Larcher, T., Tesson, L., Chenouard, V., Guillonneau, C., Brusselle, L., Vimond, N., Rouger, K., et al. (2019). Immunophenotype of a Rat Model of Duchenne's Disease and Demonstration of Improved Muscle Strength After Anti-CD45RC Antibody Treatment. Front. Immunol. *10*, 2131. https://doi.org/10.3389/fimmu.2019.02131.

17. Besnard, M., Sérazin, C., Ossart, J., Moreau, A., Vimond, N., Flippe, L., Sein, H., Smith, G.A., Pittaluga, S., Ferré, E.M.N., et al. (2022). Anti-CD45RC antibody immunotherapy prevents and treats experimental autoimmune polyendocrinopathy–candidiasis–ectodermal dystrophy syndrome. J. Clin. Invest. *132*, e156507. https://doi.org/10.1172/JCI156507.

18. Beers, S.A., Glennie, M.J., and White, A.L. (2016). Influence of immunoglobulin isotype on therapeutic antibody function. Blood *127*, 1097–1101. https://doi.org/10.1182/blood-2015-09-625343.

19. Gaston, R.S., Deierhoi, M.H., Patterson, T., Prasthofer, E., Julian, B.A., Barber, W.H., Laskow, D.A., Diethelm, A.G., and Curtis, J.J. (1991). OKT3 first-dose reaction: Association with T cell subsets and cytokine release. Kidney Int. *39*, 141–148. https://doi.org/10.1038/ki.1991.18.

20. de Romeuf, C., Dutertre, C.-A., Le Garff-Tavernier, M., Fournier, N., Gaucher, C., Glacet, A., Jorieux, S., Bihoreau, N., Behrens, C.K., Béliard, R., et al. (2008). Chronic lymphocytic leukaemia cells are efficiently killed by an anti-CD20 monoclonal antibody selected for improved engagement of FcγRIIIA/CD16. Br. J. Haematol. *140*, 635–643. https://doi.org/10.1111/j.1365-2141.2007.06974.x.

21. Cleary, K.L.S., Chan, H.T.C., James, S., Glennie, M.J., and Cragg, M.S. (2017). Antibody Distance from the Cell Membrane Regulates Antibody Effector Mechanisms. J. Immunol. *198*, 3999–4011. https://doi.org/10.4049/jimmunol.1601473.

22. Crook, M. (1993). The determination of plasma or serum sialic acid. Clin. Biochem. *26*, 31–38. https://doi.org/10.1016/0009-9120(93)90014-W.

23. Albanesi, M., and Daëron, M. (2012). The interactions of therapeutic antibodies with Fc receptors. Immunol. Lett. *143*, 20–27. https://doi.org/10.1016/j.imlet.2012.02.005.

24. Petersone, L., Edner, N.M., Ovcinnikovs, V., Heuts, F., Ross, E.M., Ntavli, E., Wang, C.J., and Walker, L.S.K. (2018). T Cell/B Cell Collaboration and Autoimmunity: An Intimate Relationship. Front. Immunol. *9*, 1941. https://doi.org/10.3389/fimmu.2018.01941.

25. Schlöder, J., Shahneh, F., Schneider, F.-J., and Wieschendorf, B. (2022). Boosting regulatory T cell function for the treatment of autoimmune diseases – That's only half the battle. Front. Immunol. *13*, 973813. https://doi.org/10.3389/fimmu.2022.973813.

26. Bruhns, P. (2012). Properties of mouse and human IgG receptors and their contribution to disease models. Blood *119*, 5640–5649. https://doi.org/10.1182/blood-2012-01-380121.

27. Leipold, D., and Prabhu, S. (2019). Pharmacokinetic and Pharmacodynamic Considerations in the Design of Therapeutic Antibodies. Clin. Transl. Sci. *12*, 130–139. https://doi.org/10.1111/cts.12597.

28. Crescioli, S., Kaplon, H., Chenoweth, A., Wang, L., Visweswaraiah, J., and Reichert, J.M. (2024). Antibodies to watch in 2024. mAbs *16*, 2297450. https://doi.org/10.1080/19420862.2023.2297450.

29. Blümich, S., Zdimerova, H., Münz, C., Kipar, A., and Pellegrini, G. (2021). Human CD34 $^{+}$ Hematopoietic Stem Cell–Engrafted NSG Mice: Morphological and Immunophenotypic Features. Vet. Pathol. *58*, 161–180. https://doi.org/10.1177/0300985820948822.

30. Thompson, S.A.J., Jones, J.L., Cox, A.L., Compston, D.A.S., and Coles, A.J. (2010). B-Cell Reconstitution and BAFF After Alemtuzumab (Campath-1H) Treatment of Multiple Sclerosis. J. Clin. Immunol. *30*, 99–105. https://doi.org/10.1007/s10875-009-9327-3.

31. Jones, J.L., Phuah, C.-L., Cox, A.L., Thompson, S.A., Ban, M., Shawcross, J., Walton, A., Sawcer, S.J., Compston, A., and Coles, A.J. (2009). IL-21 drives secondary autoimmunity in patients with multiple sclerosis, following therapeutic lymphocyte depletion with alemtuzumab (Campath-1H). J. Clin. Invest. *119*, 2052–2061. https://doi.org/10.1172/JCI37878.

32. Dörr, J., and Baum, K. (2016). Alemtuzumab in the treatment of multiple sclerosis: patient selection and special considerations. Drug Des. Devel. Ther. *10*, 3379–3386. https://doi.org/10.2147/DDDT.S97956.

33. Sim, J.H., Han, S.S., Lee, D.-S., Kim, Y.S., Lee, H., and Kim, H.-R. (2020). Analysis of Immune Cell Repopulation After Anti-thymocyte Globulin Administration for Steroid-Resistant T-cell–mediated Rejection. Transpl. Proc. *52*, 759–766. https://doi.org/10.1016/j.transproceed.2020.01.013.

34. Bosch, M., Dhadda, M., Hoegh-Petersen, M., Liu, Y., Hagel, L.M., Podgorny, P., Ugarte-Torres, A., Khan, F.M., Luider, J., Auer-Grzesiak, I., et al. (2012). Immune reconstitution after anti-thymocyte globulin-conditioned hematopoietic cell transplantation. Cytotherapy *14*, 1258–1275. https://doi.org/10.3109/14653249.2012.715243.

35. Ogonek, J., Kralj Juric, M., Ghimire, S., Varanasi, P.R., Holler, E., Greinix, H., and Weissinger, E. (2016). Immune Reconstitution after Allogeneic Hematopoietic Stem Cell Transplantation. Front. Immunol. *7*, 507. https://doi.org/10.3389/fimmu.2016.00507.

36. Thomas, M.L., and Lefrançois, L. (1988). Differential expression of the leucocyte-common antigen family. Immunol. Today *9*, 320–326. https://doi.org/10.1016/0167-5699(88)91326-6.

37. Cox, K.M., Sterling, J.D., Regan, J.T., Gasdaska, J.R., Frantz, K.K., Peele, C.G., Black, A., Passmore, D., Moldovan-Loomis, C., Srinivasan, M., et al. (2006). Glycan optimization of a human monoclonal antibody in the aquatic plant Lemna minor. Nat. Biotechnol. *24*, 1591–1597. https://doi.org/10.1038/nbt1260.

38. Schuster, M., Umana, P., Ferrara, C., Brünker, P., Gerdes, C., Waxenecker, G., Wiederkum, S., Schwager, C., Loibner, H., Himmler, G., and Mudde, G.C. (2005). Improved Effector Functions of a Therapeutic Monoclonal Lewis Y-Specific Antibody by Glycoform Engineering. Cancer Res. *65*, 7934–7941. https://doi.org/10.1158/0008-5472.CAN-04-4212.

39. Kircheis, R., Halanek, N., Koller, I., Jost, W., Schuster, M., Gorr, G., Hajszan, K., and Nechansky, A. (2012). Correlation of ADCC activity with cytokine release induced by the stably expressed, glyco-engineered humanized Lewis Y-specific monoclonal antibody MB314. mAbs *4*, 532–541. https://doi.org/10.4161/mabs.20577.

40. Wing, M.G., Moreau, T., Greenwood, J., Smith, R.M., Hale, G., Isaacs, J., Waldmann, H., Lachmann, P.J., and Compston, A. (1996). Mechanism of first-dose cytokine-release syndrome by CAMPATH 1-H: involvement of CD16 (FcgammaRIII) and CD11a/CD18 (LFA-1) on NK cells. J. Clin. Invest. *98*, 2819–2826. https://doi.org/10.1172/JCI119110.

41. Tax, W.J., Tamboer, W.P., Jacobs, C.W., Frenken, L.A., and Koene, R.A. (1997). Role of polymorphic Fc receptor FcgRIIa in cytokine release and adverse effects of murine IgG1 anti-CD3/T cell receptor antibody (WT31)1. Transplantation *63*, 106–112. https://doi.org/10.1097/00007890-199701150-00020.

42. Winkler, U., Jensen, M., Manzke, O., Schulz, H., Diehl, V., and Engert, A. (1999). Cytokine-release syndrome in patients with B-cell chronic lymphocytic leukemia and high lymphocyte counts after treatment with an anti-CD20 monoclonal antibody (rituximab, IDEC-C2B8). Blood *94*, 2217–2224.

43. Hermiston, M.L., Xu, Z., and Weiss, A. (2003). CD45: a critical regulator of signaling thresholds in immune cells. Annu. Rev. Immunol. *21*, 107–137. https://doi.org/10.1146/annurev.immunol.21.120601.140946.

44. Trowbridge, I.S., and Thomas, M.L. (1994). CD45: An Emerging Role as a Protein Tyrosine Phosphatase Required for Lymphocyte Activation and Development. Annu. Rev. Immunol. *12*, 85–116. https://doi.org/10.1146/annurev.iy.12.040194.000505.

45. Johnson, K.G., Bromley, S.K., Dustin, M.L., and Thomas, M.L. (2000). A supramolecular basis for CD45 tyrosine phosphatase regulation in sustained T cell activation. Proc. Natl. Acad. Sci. USA *97*, 10138–10143. https://doi.org/10.1073/pnas.97.18.10138.

46. Jefferis, R. (2009). Glycosylation as a strategy to improve antibody-based therapeutics. Nat. Rev. Drug Discov. *8*, 226–234. https://doi.org/10.1038/nrd2804.

47. Shultz, L.D., Brehm, M.A., Garcia-Martinez, J.V., and Greiner, D.L. (2012). Humanized mice for immune system investigation: progress, promise and challenges. Nat. Rev. Immunol. *12*, 786–798. https://doi.org/10.1038/nri3311.

48. Vély, F., Barlogis, V., Vallentin, B., Neven, B., Piperoglou, C., Ebbo, M., Perchet, T., Petit, M., Yessaad, N., Touzot, F., et al. (2016). Evidence of innate lymphoid cell redundancy in humans. Nat. Immunol. *17*, 1291–1299. https://doi.org/10.1038/ni.3553.

49. Mace, E.M., and Orange, J.S. (2016). Genetic Causes of Human NK Cell Deficiency and Their Effect on NK Cell Subsets. Front. Immunol. *7*, 545. https://doi.org/10.3389/fimmu.2016.00545.

50. Krzywinska, E., Cornillon, A., Allende-Vega, N., Vo, D.-N., Rene, C., Lu, Z.-Y., Pasero, C., Olive, D., Fegueux, N., Ceballos, P., et al. (2016). CD45 Isoform Profile Identifies Natural Killer (NK) Subsets with Differential Activity. PLoS One *11*, e0150434. https://doi.org/10.1371/journal.pone.0150434.

51. Hesslein, D.G.T., Takaki, R., Hermiston, M.L., Weiss, A., and Lanier, L.L. (2006). Dysregulation of signaling pathways in CD45-deficient NK cells leads to differentially regulated cytotoxicity and cytokine production. Proc. Natl. Acad. Sci. USA *103*, 7012–7017. https://doi.org/10.1073/pnas.0601851103.

52. Krzywinska, E., Allende-Vega, N., Cornillon, A., Vo, D.-N., Cayrefourcq, L., Panabieres, C., Vilches, C., Déchanet-Merville, J., Hicheri, Y., Rossi, J.-F., et al. (2015). Identification of Anti-tumor Cells Carrying Natural Killer (NK) Cell Antigens in Patients With Hematological Cancers. EBioMedicine *2*, 1364–1376. https://doi.org/10.1016/j.ebiom.2015.08.021.

53. Hesslein, D.G.T., Palacios, E.H., Sun, J.C., Beilke, J.N., Watson, S.R., Weiss, A., and Lanier, L.L. (2011). Differential requirements for CD45 in NK-cell function reveal distinct roles for Syk-family kinases. Blood *117*, 3087–3095. https://doi.org/10.1182/blood-2010-06-292219.

54. Merino, A., Zhang, B., Dougherty, P., Luo, X., Wang, J., Blazar, B.R., Miller, J.S., and Cichocki, F. (2019). Chronic stimulation drives human NK cell dysfunction and epigenetic reprograming. J. Clin. Invest. *129*, 3770–3785. https://doi.org/10.1172/JCI125916.

55. Miller, M.L., and Finn, O.J. (2020). Flow cytometry-based assessment of direct-targeting anti-cancer antibody immune effector functions. In Methods in Enzymology (Elsevier), pp. 431–456. https://doi.org/10.1016/bs.mie.2019.07.026.